TABLE OF CONTENTS

	Page	
I. SUMMARY	1	1/A6
II. INTRODUCTION	3	1/A8
III. COMPOSITE CONDUCTOR PROPERTIES , SPECIMENS , AND EQUIPMENT	5	1/A10
IV. QUENCH REGIMES OF SINGLE SPECIMENS AND RELATED RESULTS	13	1/B4
V. QUENCH ONSET OF THE CONDUCTOR BUNDLE AND RELATED PHENOMENA	46	1/E10
VI . COOLDOWN OF COMPOSITE CONDUCTORS FROM POST-QUENCH CONDITIONS	55	1/F6
VII. FORCED FLOW EFFECTS	66	1/G8
VIII. CONCLUSIONS	74	2/A7
APPENDIX A . EXPERIMENTAL DATA	80	2/A13

NASA Contractor Report 3262

Cryogenic-Coolant He^4-Superconductor Dynamic and Static Interactions

S. Caspi, C. Chuang, Y. I. Kim,
R. J. Allen, and T. H. K. Frederking

GRANT NSG-3153
APRIL 1980

NASA

NASA Contractor Report 3262

Cryogenic-Coolant He^4-Superconductor Dynamic and Static Interactions

S. Caspi, C. Chuang, Y. I. Kim,
R. J. Allen, and T. H. [illegible] Fredericking
University of California at Los Angeles
Los Angeles, California

Prepared for
Lewis Research Center
under Grant NSG-3153

National Aeronautics
and Space Administration

**Scientific and Technical
Information Office**

1980

BLANK PAGE

TABLE OF CONTENTS

	Page
I. SUMMARY	1
II. INTRODUCTION	3
III. COMPOSITE CONDUCTOR PROPERTIES , SPECIMENS , AND EQUIPMENT	5
IV. QUENCH REGIMES OF SINGLE SPECIMENS AND RELATED RESULTS	13
V. QUENCH ONSET OF THE CONDUCTOR BUNDLE AND RELATED PHENOMENA	46
VI . COOLDOWN OF COMPOSITE CONDUCTORS FROM POST-QUENCH CONDITIONS	55
VII. FORCED FLOW EFFECTS	66
VIII. CONCLUSIONS	74
APPENDIX A . EXPERIMENTAL DATA	80

I. SUMMARY

This report summarizes the second and final phase of investigations conducted under NASA Grant NSG 3153 concerned with cryogenic coolant He^4 - superconductor interaction. The first phase, with emphasis on quasi-steady quench and post-quench phenomena, dealt with several properties of the solid and composite superconductor - He^4 interaction. In particular the behavior of the coated conductor was studied from the thermodynamic critical temperature down to He II temperatures, and at pressures from the saturated vapor pressure up to 10 bar. An important result of the first phase of the studies had been the significance of the ratio of the applied formvar thickness d_{FV} to the thermodynamic limiting thickness δ_L associated with the state of the fluid. The latter thickness δ_L has been a strong function of temperature,and mostly smaller than d_{FV} in the range covered. An exception is the vicinity of the lambda transition on the He I side at which the applied d_{FV} was equal to δ_L .

In the second phase the importance of the thickness ratio was confirmed during cooldown from post-quench conditions . The time needed for recovery of superconductivity from high initial metal temperatures was found to be closely related to (d_{FV}/δ_L) . Emphasizing the advantages created by application of coatings we summarize the most important findings by referring to the following points:

a. Coatings are beneficial for values $(d_{FV}/\delta_L) > 1$ by pushing disturbances created by boiling mode changes toward high metal temperatures;

b. Associated with coatings in the range $(d_{FV}/\delta_L) > 1$ is the creation of a post-quench regime (B) with efficient liquid-solid contact ;

c. Favorable values of $(d_{FV}/\delta_L) > 1$ were found between 3 and 4 K in liquid He I, and below the lambda transition in superfluid liquid He II . This results in high metal temperatures

at the upper boundary of post-quench regime B.Therefore, a magnet of the category and specification considered should be operated only at these favorable bath temperatures.

d. Times τ needed for recovery of superconductivity from metal temperatures in post-quench regime B were found to be considerably shorter than for bare conductors.

e. Even for cooldown from the film boiling post-quench regime which was above 40 K, in a range beyond regime B, the coated conductor showed no deterioration of recovery times. On the contrary, there was a slight reduction in τ because of the application of the coatings.

Thus, coatings have been found to be very beneficial provided certain requirements are met . It is necessary to design a cooling system which makes use of the latent heat of vaporization of He^4 . Further, the winding system should be fluid-ventilated as fully as possible. Finally, for a particular application the disturbance spectrum causing quenches (e.g. magneto-mechanical friction) should be known in order to make optimum use of the coatings.

II. INTRODUCTION

The second phase of the composite superconductor evaluation followed up closely on previous investigations (Phase I of cryogenic-coolant He^4-superconductor interaction) of various specimens of NbTi-Cu coated with formvar. This work has been detailed in Reference 1. The composite conductor containing type II filaments of the alloy Nb-48-Ti had been selected by NASA (Lewis Research Center, Cleveland) for development work in conjunction with MHD generator systems. Many transport properties of interest in conjunction with superconductor coolant interaction were unknown in the beginning of the research (Summer 1977). Motivation for use of formvar and accumulation of this type of data has arisen primarily from the need for efficient quench protection of magnets, originally thought to be in the area of safe dielectric conditions. Furthermore, superconducting equipment of intermediate and high energy density is potentially an attractive choice not only for MHD, but also for other energy systems, such as inductive energy storage, superconducting motors and generators, and fusion reactors. In the fusion area, however, not all conceptual designs proposed in recent years utilize considerable energy densities of the magnets. On the contrary, very conservative design criteria appear to prevail in order to incorporate the largest possible safety factors based on simple criteria of quasi-steady transport. Power plants with superconducting subsystems for mobile equipment and energy converters, however, may have to meet demands for more compact designs and less conservative criteria. An example of recent developments in this area has been described in Reference 2. The highest energy densities have been achieved in broad application areas of small laboratory solenoids for various purposes. Approaches are usually not quantified and evolution appears to have taken place primarily on the basis of trial and error approaches. For the large magnets of the future however a much closer look at quantitative details appears to be necessary. In particular very little information has been reported in the early development of various superconductive composites on the effect of insulators on quench protection and stabilization. The need for this information seems to be not in great doubt in view of the magnet configuration visualized for NASA MHD magnet work.

For the NASA MHD magnet, a winding technique employing turn to turn insulation by formvar, and separation of turns by G-10 epoxy glass laminate

slats (thickness 1/64 in ≃ 0.04 cm) is of interest. This system of spacers with about 1/3 cm spacing and spacer width of about 0.16 cm allows passage of the coolant (He^4) between layers. Since the proposed MHD magnet system incorporates various winding and spacer orientations with respect to gravity, there may be favorable and unfavorable positions in gravitational convection. As an alternate solution, the use of He II has been envisioned with a lack of gravitational problems encountered during single-phase liquid operation. However, the phase boundaries of He II are narrow, and other problems may arise during two-phase and triple-phase flow. In the light of these requirements, the first phase of this research has focused considerable attention on quasi-steady transport conditions encountered with single composite superconductivity specimens in pool arrangements. These formvar-coated conductors were subjected to quenches from the superconducting to the normal state by a heater simulation technique. Results are readily assessed on the basis of special quench and post-quench heat flux densities (dissipated power densities at the surface of the conductor, i.e. at the formvar-fluid interface). The type of graphical representation used may be referred to as "quench diagram". For each particular thermodynamic trajectory in the fluid a set of quench functions and post-quench functions pertains to a specific composite. These quench diagrams in turn may form the basis for a classification of transient phenomena supplemented by the knowledge of "pure" heat transfer regimes known from classical texts. For complex geometries, such as bundles of conductors, more complicated conditions may arise while dominant features of the quench diagrams are retained in a certain range of parameters. These various topics supplemented by forced flow information will be discussed subsequently as outlined in the table of contents.

III. COMPOSITE CONDUCTOR PROPERTIES, SPECIMENS, AND EQUIPMENT

Conductor Properties. Significant properties of the composite have been obtained previously. For easy access to dimensions and other quantities, Table III.1 contains basic data reproduced from Ref.1. A major point to be considered for data interpretation is the wide tolerance in the formvar coating thickness (d_{FV}), and departures from an ideal cross sectional geometry (base square area a^2 with a radius of curvature R_c at the rounded edges of the composite). These tolerances cause uncertainties for comparisons of various results which involve surface areas of the formvar and cross sectional areas available to the fluid.

Another point is the uncertainty in the transition temperature T_{sn} at the phase change from the superconducting to the normal state. Various filaments have different T_{sn}-values. As the specimen preparation did not avoid entirely some damage to the interior filaments, T_{sn} - values "seen" by the various interior carbon resistance thermometers changed from one specimen to the next. The transition temperature quoted in Table III.1 is an average of data collected during the first phase of the studies.

Several transport properties have been determined previously, in particular thermal conductivities. For details we refer to Reference 1, and note that an effective thermal conductivity of formvar will be discussed below in some length in the context of quench onset prediction.

Specimens. For easy reference the specimen list of Reference 1 is reproduced in part. Single specimens are listed in Table III.2, and further properties of the bundle of conductors are outlined subsequently.

The single specimens (IS series) have been augmented by two more samples (IS-4 and IS-5). The fourth individual specimen IS-4 was used to minimize heat leaks. Therefore no carbon thermometer was incorporated. Copper resistance thermometry employed above 20 K had the purpose of resolving details of the post-quench recovery of the superconducting state. Also peak heat flux data and quench onset results

TABLE III . 1

COMPOSITE PARAMETERS (Nb-Ti-Cu-FORMVAR)

Total cross section of the composite	A_{tot} , cm^2	4.80×10^{-2}
Circumference of the composite	C_c , cm^2/cm	0.81
Cu-cross section	A_{cu} , cm^2	0.033
Insulator (formvar) thickness	d_{FV} , μm	30
Type II filament diameter	$\bar{D}_F$, cm	0.018
Conductor thickness	a , cm	0.22_4
Radius of curvature at conductor edges	R_c , cm	0.05
Transition temperature at inner surface	T_{sn} , K	8.5_6
Transition temperature of filament	T_{sn} , K	8.9

IDEAL CIRCUMFERENCE: $C_c = 4a + 2\pi R_c - 8 R_c$

IDEAL TOTAL CROSS SECTION: $A_{tot} = a^2 - R_c^2(4 - \pi)$

TABLE III. 2

SPECIMENS

DESIGNATION	POSITION	LENGTH OF TEST SECTION	REMARKS
IS-1	AXIS : HORIZONTAL; "DIAMOND" CROSS SECTION	2.17 cm	WETTED AREA: 1.74_9 cm^2
IS-1S	SAME AS IS-1		COMPOSITE INSTRUMENTED AS RESISTANCE THERMOMETER
IS-1B	SAME AS IS-1		FORMVAR REMOVED; AREA : 1.73 cm^2
IS-2	AXIS : HORIZONTAL; CROSS SECTION	2.40 cm	MOUNTED IN PHENOLIC; TOP AREA WETTED: 0.483_6 cm^2
IS-3A/B	AXIS : HORIZONTAL; "DIAMOND"	1.95 cm	VACUUM INSULATION; 1.71 cm^2 A: Pt-10 % Rh; B: CONSTANTAN HEATER
IS-4	AXIS; HORIZONTAL; "SQUARE"-POSITION	2.38 cm	WITHOUT C-THERMOMETER
IS-5	AXIS: HORIZONTAL; "SQUARE" POSITION	2.36 cm	WITHOUT C-THERMOMETER ; BARE SPECIMEN

ALL SPECIMENS ARE FORMVAR - COATED UNLESS NOTED OTHERWISE.

were evaluated with specimen IS-4 . The fifth sample IS-5 had no formvar coating . This "bare " sample served as reference case for several composite quantities. The conductor was used as"received" . Prior to immersion in liquid He^4 the surface was rinsed with acetone and ethanol. There exists an oxide layer and impurity layer respectively on the surface of bare copper wire at the end of the drawing process. In addition, exposure to the air of metropolitan areas permits further impurity accumulation during a longer period of time. Thus, despite a shiny surface , there is an impurity layer whose thickness may be significantly below the wave length of light, i.e, below the order of 0.5 μm. Details of this surface layer were not investigated.

The bundle of nine composite conductors has been described in Reference 1. Figure III.1 shows schematically the top view for a horizontal orientation of the spacer-duct system (or side view for the vertical spacer-duct system). Figure III.2 is a sketch of the cross section of the bundle.

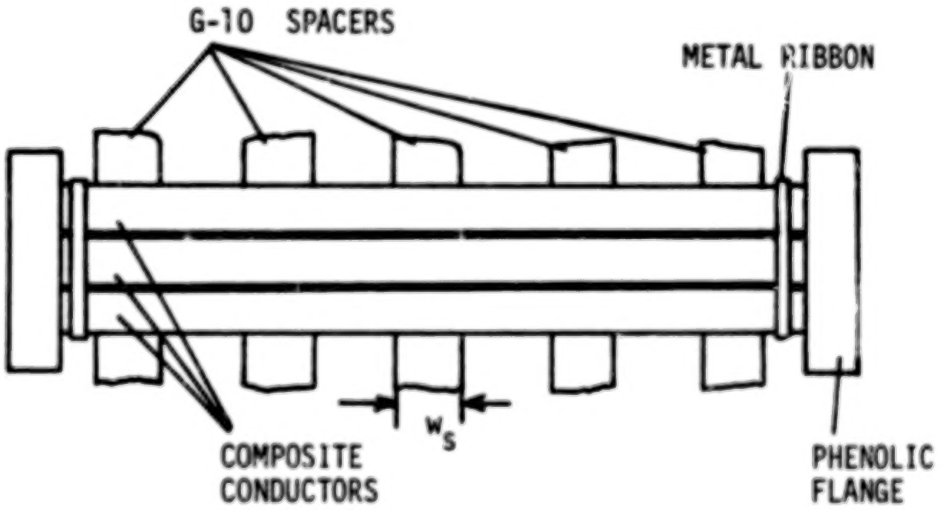

Figure III.1 . Schematic of conductor bundle

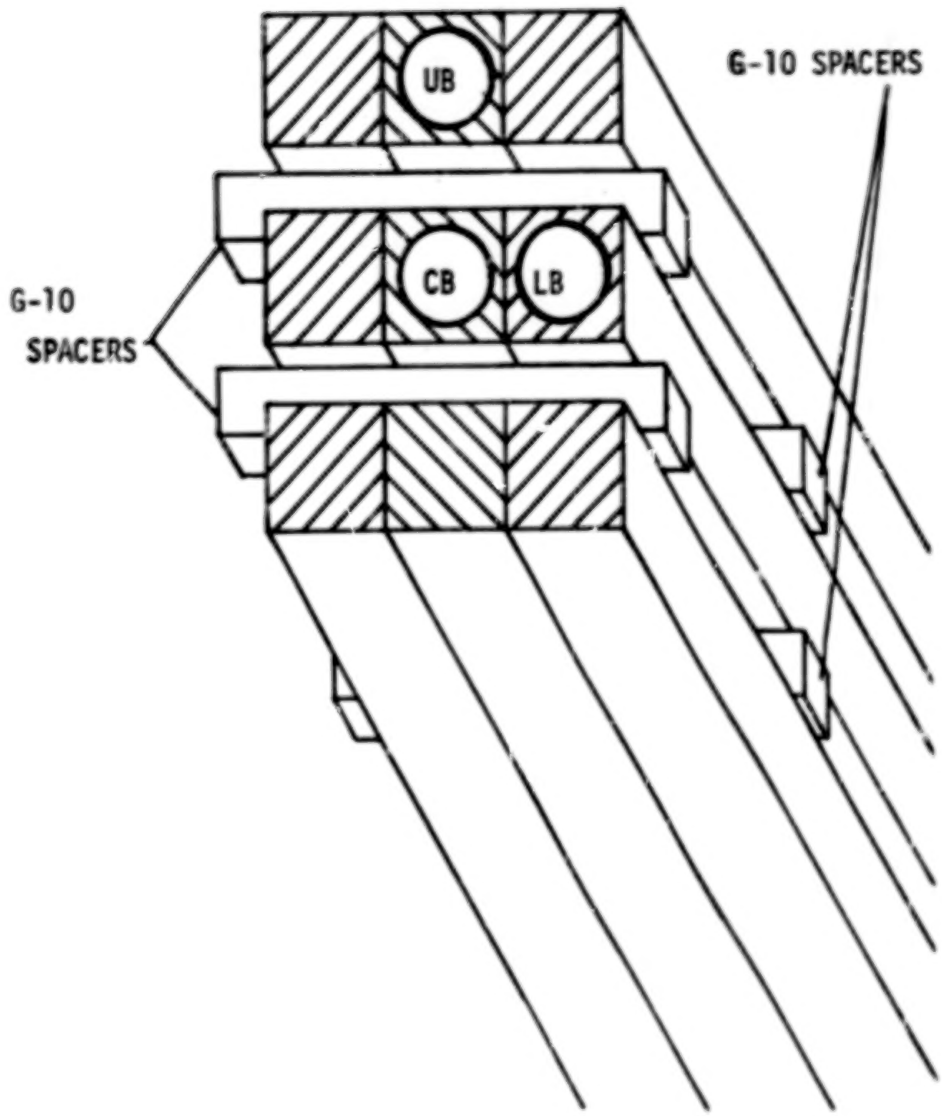

CB CENTRAL HEATED CONDUCTOR
UB UPPER CONDUCTOR (WITH THERMOMETER)
LB LOWER CONDUCTOR (WITH THERMOMETER)

Figure III.2 . Cross sectional view of conductor bundle (schematic)

As described previously in Reference 1, the central conductor (CB) had been equipped with a heater and a carbon thermometer. Adjacent conductors however were not energized directly. Conductor LB had solid-solid contact with CB. This arrangement allowed considerable transfer of thermal energy, in particular when the solid-fluid interaction on fluid-wetted surfaces was characterized by low heat transfer coefficients (h_{if}). Conductor UB was separated from the central conductor row by the coolant duct formed by G-10 spacers of nominal thickness 1/64 in. $\approx$ 0.040 cm . Aside from the phenolic end sections and the constraining metal ribbon (Figure III.1) , there were five spacers of nominal width w_s = 1/16 in. $\approx$ 0.16 cm with a gap of 1/8 in. $\approx$ 0.32 cm left in between consecutive spacers . In the subsequent discussion two main sets of thermal resistances of the bundle are separated by use of a simplified thermal circuit. Though no exact areas are known because of the various tolerances mentioned, we note that a perfectly plane face of the conductor has a contact area between CB and LB of $(A_2/2)$ which is the product of $(a - 2 R_c)$ and the conductor length L. Accordingly, the entire central conductor has an ideal contact area of

$$A_2 = 2 L (a - 2 R_c) \qquad \text{(III.1)}$$

with $A_2 = 0.538$ cm^2. The total surface area of the unobstructed central conductor is the product of its circumference C_c and the length L . However at spacer locations efficient thermal transport is prevented . Therefore, to first order, the diathermic area of the central conductor CB is

$$A_{tot} = C_c L - 2 N_s w_s (a - 2 R_c) \qquad \text{(III.2)}$$

for N_s spacers ($N_s = 5$). We obtain $A_{tot} = 1.563$ cm^2. The fluid-wetted area A_1 will be

$$A_1 = A_{tot} - A_2 \qquad \text{(III.3)}$$

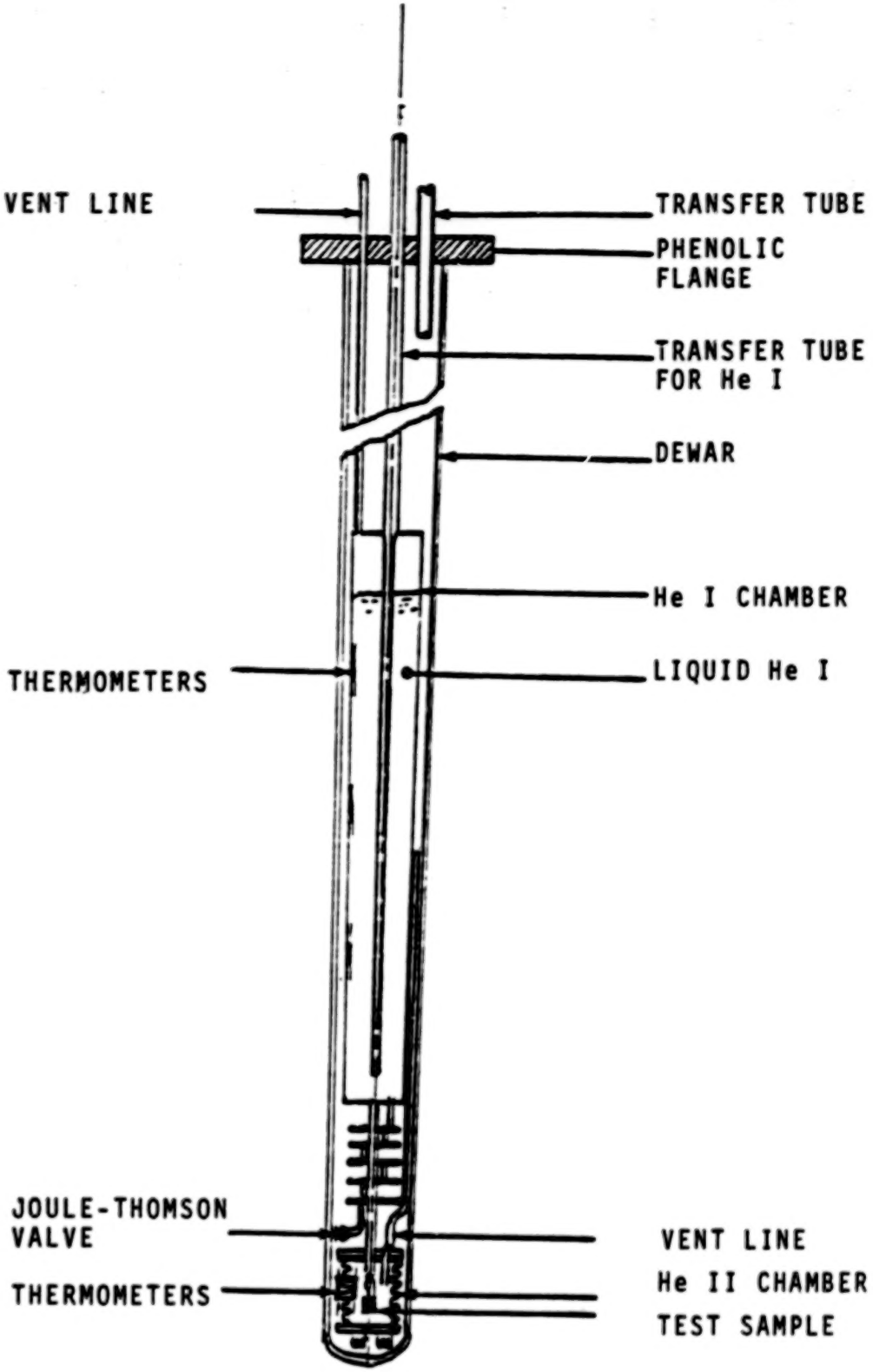

Figure III.3 . Schematic of He I- He II System

with $A_1 = 1.025$ cm^2 . Previous bundle results reported in Reference 1 have been normalized in terms of the nominal fluid wetted area of CB. Therefore, we list dissipated energies per total diathermic area A_{tot} in the present report (Appendix A) . Additional data obtained during the present phase II of the composite evaluation have been listed also in Appendix A . Details of the thermal circuit for the bundle are discussed in Section IV.2 .

Equipment. The various cryostat components(including the pressurized helium system) have been outlined in the previous report (Reference 1). For work near 1 bar it is convenient to employ a He I - He II hybrid system in a suitable modification. Several versions of these systems have been reported in the literature (Reference 3). The system constructed is shown schematically in Figure III.3. Major portions of the system are the upper He I chamber , the lower He II chamber for superfluid operation , and interconnecting plumbing , such as heat exchangers and throttling valve.

IV. QUENCH REGIMES OF SINGLE SPECIMENS AND RELATED RESULTS

A quench diagram with thermodynamic trajectories starting from near-saturated liquid He^4 is presented in Figure IV.1 . This figure plots data primarily of specimen IS-4 and in part of IS-1 (both formvar-coated). Prior to the solid state phase change called quench, the pre-quench regime A is established at a heat flux density $q < q_o$. The function q_o signals quench onset at various bulk fluid temperatures. Aside from a distinct change at the lambda transition temperature (T_λ) , q_o appears to be a monotonically decreasing function of the fluid temperature T_b of the near-saturated liquid He^4 . At $q > q_o$, two post-quench regimes may occur. The first regime B is established prior to a switch in thermal boundary conditions toward the onset of film boiling ($q = q_p$). Accordingly, for $q_0 < q < q_p$ liquid contacts the solid ,i.e. the formvar surface. This implies efficient cooling conditions. Therefore, post-quench regime B appears to be beneficial from the point of view of sufficiently safe, passive quench protection measures. At the peak heat flux density q_p ,post-quench regime C begins . The addition of an insulating vapor film to the existing thermal resistances produces very unfavorable cooling conditions. Obviously any severe quench to $q > q_p$ may lead to considerable temperature excursions if regime C is reached. It may be expected that slow recovery will take place. For the latter it is presumed that the cause of dissipation has been removed after a certain time interval. Figure IV.1 shows a strong variation of q_p with T_b . The present formvar coating is sufficiently thick to provide a rather broad regime B in two thermodynamic ranges. The first one is the vicinity of the normal boiling point including the broad maximum of q_p, and the second one is the He II regime around 2 K,(vicinity of another maximum of q_p). In contrast, near the lambda transition from He I to He II the two functions come so close together that regime B is practically eliminated . (It is noted that most curves in Figure IV.1 have been drawn to guide the eye. An exception is the dashed curve representing the Soloski equation for single specimens in a pool of He II. This function has been referred to in Reference 1).

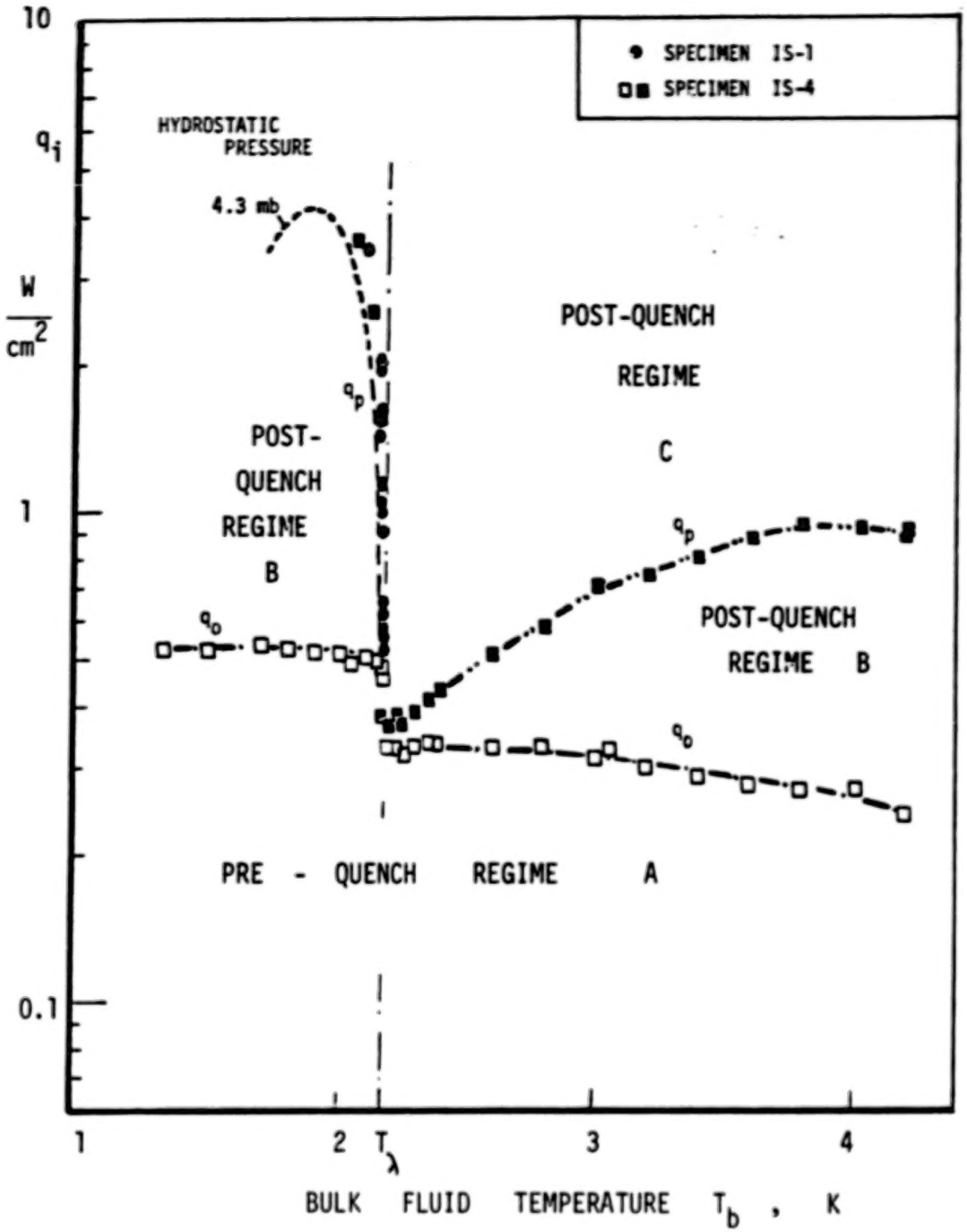

Figure IV.1 . Quench regimes characterized by heat flux densities q_i;
i = o quench onset ;
i = p "peak" value at onset of film boiling

For the vicinity of T_λ a detailed set of data has been plotted in Figure IV.2 which includes recovery results. We turn subsequently to further details of various phenomena related to the quench diagram. The topics considered are quench onset , peak flux functions , influence of insulating coatings, and conductor length influence for the long single conductor in a pool with a local dissipative section.

Quench Onset. The onset heat flux density q_o is reached when the thermal resistance system permits heating of the type II filaments to the transition temperature T_{sn} .We consider a slab geometry at quasi-steady conditions for a simplified treatment . A circuit with thermal resistances in series is adopted as shown schematically in Figure IV.3 .

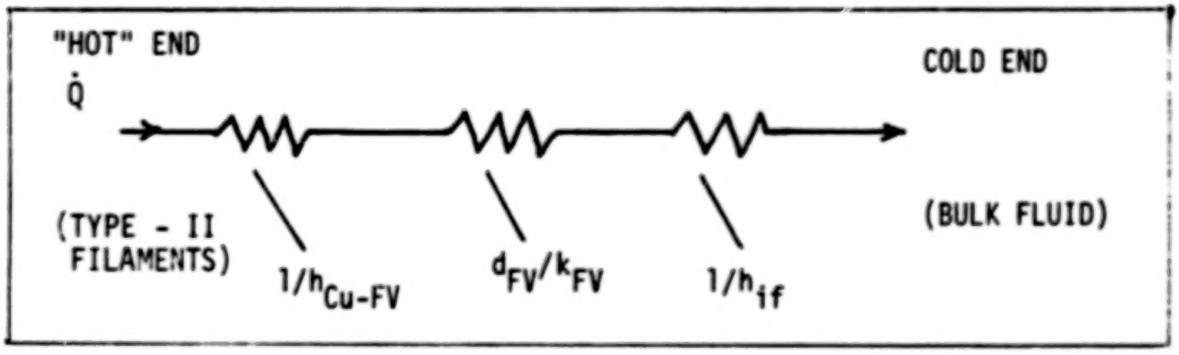

Figure IV.3. Simplified thermal circuit

The contact conductance (Kapitza conductance) from copper to formvar is designated as h_{Cu-FV} (= heat transfer coefficient) . The specific re - sistance of the formvar layer is the ratio of thickness d_{FV} to the thermal conductivity k_{FV} of formvar. Further h_{if} is the heat transfer coefficient from the insulator to the fluid which expresses the generally non-linear interaction between solid and coolant.. The overall heat transfer coefficent $\bar{U}_1$ of the single specimen may be expressed as

$$1/\bar{U}_1 = 1/h_{Cu-FV} + d_{FV}/k_{FV} + 1/h_{if} \qquad \text{(IV.1)}$$

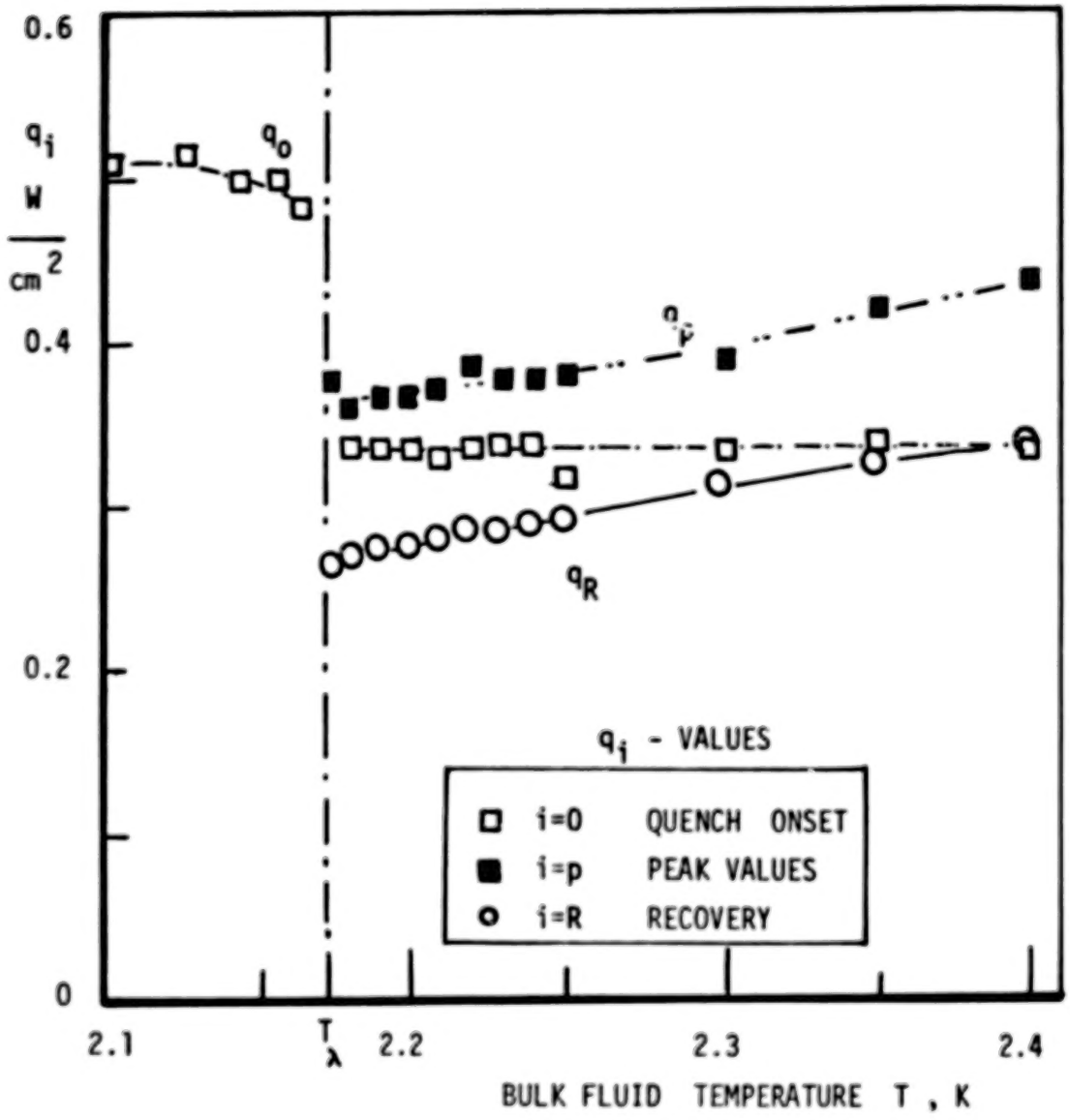

Figure IV. 2. Quench conditions near the lambda transition (He I - He II)

Making use of an effective thermal conductivity k_{eff} of the formvar and formvar-adjacent system we express Equation (IV.1) as

$$1/\bar{U}_1 = d_{FV}/k_{eff} = d_{FV} / (k_{FV}\, \phi_R) \qquad \text{(IV.2)}$$

with a reduction factor

$$\phi_R = 1 / (1 + \varepsilon_{Cu\text{-}FV} + \varepsilon_{if}) \qquad \text{(IV.3)}$$

The various contributions in the denominator of Equation (IV.3) on the right hand side are

$$\varepsilon_{Cu\text{-}FV} = (k_{FV} / d_{FV})\, h_{Cu\text{-}FV}^{-1} \qquad \text{(IV.4)}$$

and

$$\varepsilon_{if} = (k_{FV} / d_{FV})\, h_{if}^{-1} \qquad \text{(IV.5)}$$

No direct data are available for the Kapitza conductance between formvar and copper . However, metal-epoxy contacts have been investigated.(Some early results have been compared in Reference 4). It appears that $h_{Cu\text{-}FV}$ may have the order of magnitude 0.1 to 1 W cm^{-2} K^{-1} .Then for an insulator of thickness $\sim 10^{-3}$ cm, an insulator k-value of 10^{-4} W cm^{-1} K^{-1}, and the order of $h_{Cu\text{-}FV}$ quoted, we obtain a contribution $\varepsilon_{Cu\text{-}FV}$ of the order 0.1 to 1 . It is noted however that recent data reported by Matsumoto et al . (Reference 5) appear to elucidate the problem of separating insulator bulk effects from contact domain contributions. This separation seems to become more difficult when the insulator layer is quite thin.

The h_{if} -values of solid-coolant interaction may vary considerably in the T_b -range covered in Figure IV.1 . Large values are encountered during nucleate boiling with h_{fi} of the order 1 W cm^{-2} K^{-1} . Similar values appear to be possible near T_λ in He II. It is expected that the Kapitza resistance between He II and formvar may increase proportional to T_b^{-3} , however no data appear to be available to substantiate this point. In other regions and flow regimes lower values of h_{if} may be

possible. So far the thermal resistance between type II filaments and Cu has been omitted . Aside from geometry effects associated with a small heat flow cross section, there are additional thermal resistance contributions in radial direction. For a similar composite a radial thermal conductivity of the order 0.1 W cm^{-1} K^{-1} has been reported by Hust (Reference 6) . From the present specimens even lower values of effective thermal conductivities for Cu have been obtained. The latter include additional resistance contributions and geometry effects. Turning to metal-metal joints we note that Kapitza conductances close to theoretical values have been reported for pure Nb-Cu contacts (Reference 7). It is expected from the present and previous results that type II filament - Cu conductances are lower, by about one order of magnitude . These conductances h_{II-Cu} will depend on the particular manufacturing method used . In view of these constraints and conditions, we note that the effective radial k-values for Cu obtained during the first phase (Reference 1) appear to be consistent with other information for the metallic parts of the composite.

As far as the effective conductivity of formvar (Equation IV.2) is concerned we arrive at the conclusion that a reduction factor ϕ_R of Equation (IV.3) is easily possible. Thus, k_{eff} is a lower bound to k_{FV} of bulk formvar. In any case, the dominant thermal resistance of the formvar-coated composite investigated is residing in the formvar layer itself. Therefore we arrive at a prediction of q_o for quasi-steady transport by integration in radial direction

$$\int q_o \, dr = \int_{T_b}^{T_{sn}} k_{eff}(T) \, dT \qquad \text{(IV.6)}$$

The function $k_{FV}(T)$ reported in Reference 1 for the first phase of this work has been evaluated for thermodynamic and thermohydrodynamic conditions which minimize h_{if} . Therefore we have $k_{eff} \approx k_{FV} = k_{REF}(T/T_{REF})^n$ with a power law exponent n = 0.89 and a constant $k_{REF} = 4.9 \cdot 10^{-5}$ W $cm^{-1}K^{-1}$, (T_{REF} = 1 K) . The resulting quench onset function is

$$q_o = d_{FV}^{-1} \int_{T_b}^{T_{sn}} k_{FV}(T) \, dT \qquad \text{(IV.7)}$$

or

$$q_o = [k_{REF}/(n+1)]\ d_{FV}^{-1}\ [T_{sn}^{n+1} - T_b^{n+1}]/\ T_{REF}^{n} \qquad (IV.8)$$

This function has been compared with q_o-data of specimen IS-4 in Figure IV.4. Below the lambda temperature there is good agreement with data (within error margin of k_{FV}). At the lambda transition to He I additional thermal resistance is created as $1/h_{if}$ increases significantly. Therefore the q_o-data in He I are noticeably lower than in He II.

Peak Flux Functions. In He I the Kutateladse equation is a useful reference function (discussed in Reference 1). In He II no exact quantitative agreement of prediction with data could be obtained with the size and dimensions of the present single specimens (due to pumping power limitations). Three different types of equations have become known for large single specimens with diameter above the order 0.1 cm . They are listed as Equations (IV.9) ,(IV.10), and (IV.11).

Haben et al.:

$$q_p = \rho_s\ ST\ w_{eff} \quad ;$$

$$w_{eff} = C_{3H} \left\{ (\eta_n/\rho)\ S\ |\nabla T| \right\}^{1/3} \qquad (IV.9)$$

Leonard-Clermont Equation, modified for the regime of large diameters:

$$q_p = \rho_s\ S\ T\ w_{eff} \ ;$$

$$w_{eff} = C_{3LC} \left\{ (\eta_n/\rho)\ S\ |\nabla T| \right\}^{1/3} \left\{ (\rho/\rho_s)^2 (\rho/\rho_n)^2 \right\}^{1/3} \qquad (IV.10)$$

Soloski equation:

$$q_p = \rho_s\ S\ T\ w_{eff} \ ;$$

$$w_{eff} = C_{3S}\ \ (\rho_s/\rho_n)^{1/3} \left\{ (\eta_n/\rho)\ S\ |\nabla T| \right\}^{1/3} \qquad (IV.11)$$

(ρST is the thermal energy density of He II, ρ_s/ρ = superfluid density ratio, w_{eff} = effective counterflow velocity ; L_{ref} = reference length ;

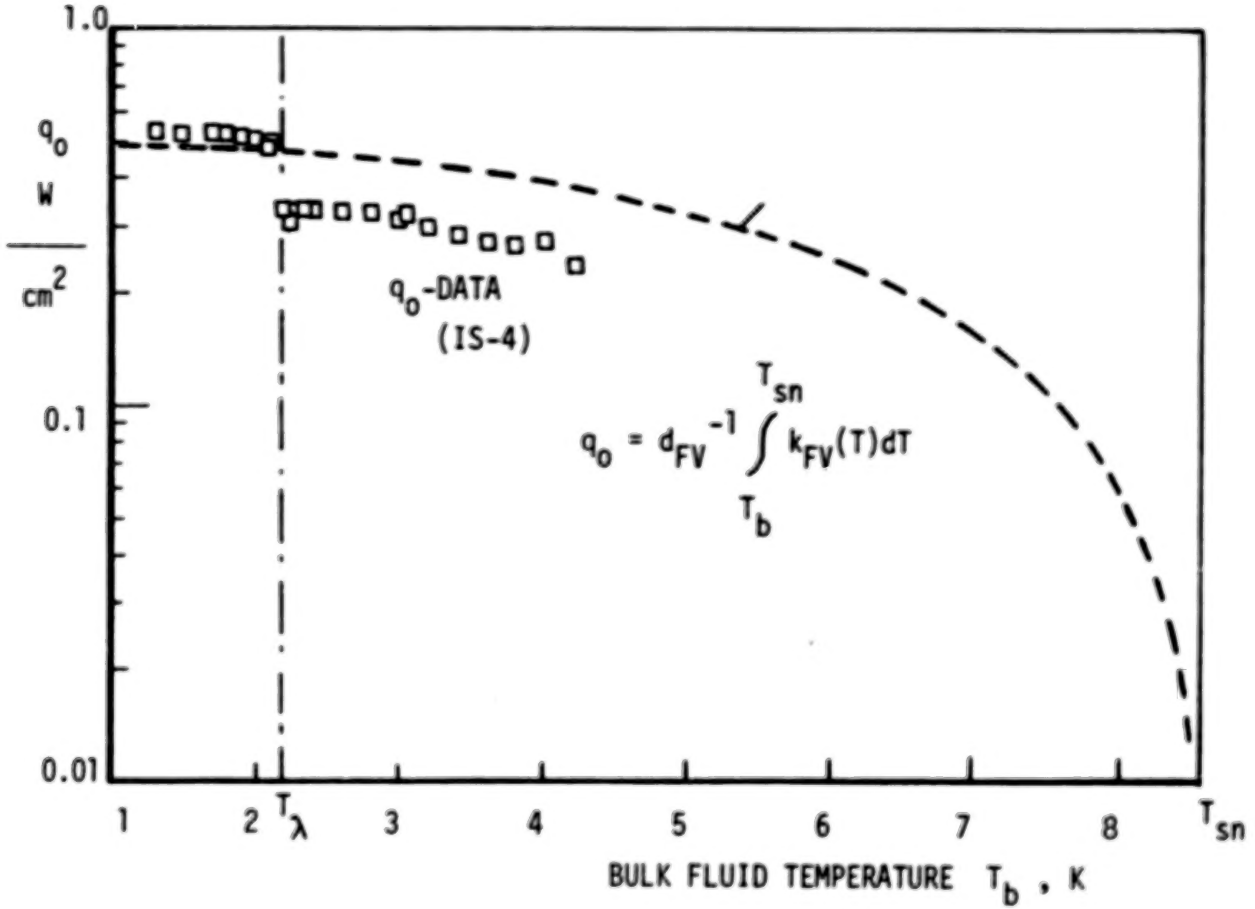

Figure IV. 4 . Comparison of quench onset data q_o with prediction (Equation IV. 8)

η_n normal fluid viscosity , ρ liquid density , ρ_n normal fluid density; S entropy per unit mass). All of these equations loose their meaning as peak flux density equation very close to the lambda transition . As T approaches T_λ , ρ_s/ρ decreases to zero, and with it q_p is predicted to become very small. The various experiments have shown that there is a continuous q_p-function with finite values at T_λ .

In the equation of Haben et al. (Reference 8) the reference length in the $|\nabla T|$ -term is the coherence distance $\xi(T)$. A simplified expression for ξ has been used : $\xi = \xi_o(\rho/\rho_s)$. Thermophysical properties are evaluated at the arithmetic mean film temperature of the disordered layer near the wall . Equation (IV.9) has been found to be a first order approximation primarily near the q_p-maximum and at temperatures above the maximum. Below the temperature of the maximum q_p values predicted appear to be above experimental data. However, at the time of publication of Reference 8 ,and even today there seem to be no data available for(a)of the order 1 cm below 1.8 K . The constants incorporated in Equation (IV.9) are expressed as $C_3 \xi_o^{-1/3} = 16 \text{ cm}^{-3}$.

The asymptotic form of the Leonard-Clermont equation has been proposed by Amar (Reference 9). The Leonard-Clermont equation (Reference 10) has covered a wide range in variables on the basis of a single power law suitably modified for the diameter influence. The modification adopted by Amar has been discussed in detail in Reference 9, and in Reference 11 further comments have been given. The properties of the modified equation (IV.10) are evaluated at the arithmetic mean temperature of the disordered He II film near the solid surface.

The Soloski equation (Reference 11) is based again on thermophysical properties at the arithmetic mean film temperature. The refe - rence length in the $|\nabla T|$-term of this equation is $L_{ref} = 1$ cm. The constant K_{3S} has the value 9.28 .

Further details of these three functions $q_p(T_b)$ are provided in

BLANK PAGE

BLANK PAGE

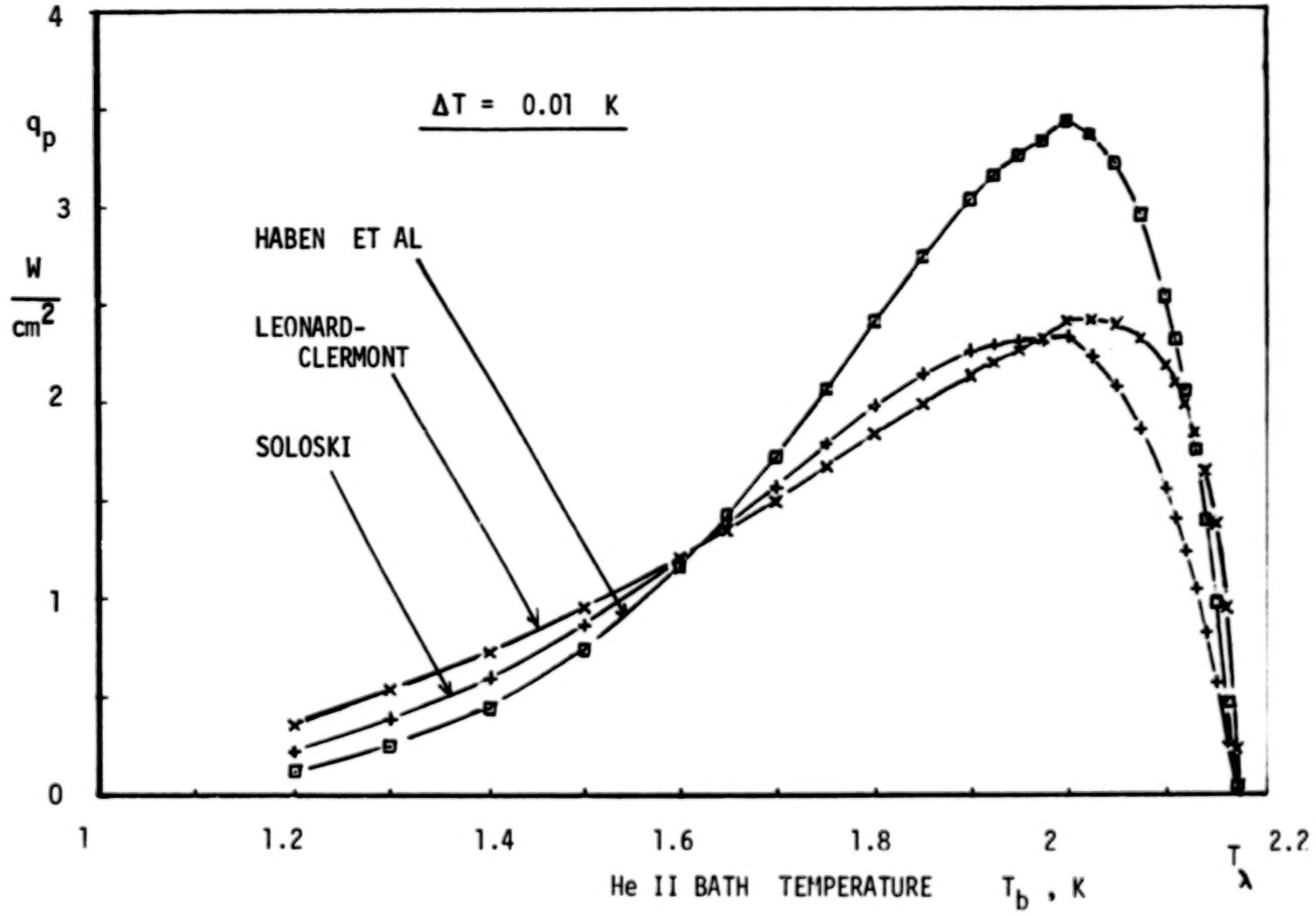

Figure IV.5. Comparison of peak heat flux density functions for He II at constant temperature difference; (Courtesy of Dr. Soloski)

Figure IV.5. The figure shows that the various q_p-functions have the common property of a maximum not too far from 2 K . The largest q_p-values are predicted by the Haben et al. equation at the maximum . However at low temperatures the modified Leonard-Clermont equation turns out to have the largest q_p .

Peak heat flux data are usually not collected at a constant temperature difference ΔT. Instead, often the hydrostatic pressure difference is controlled readily by keeping the submersion depth of the sample constant in a bath of near-saturated He II. When pressurized He II is employed however, usually an integration of the He II equations is required in order to obtain peak values. This integration has to be done for the thermodynamic path traversed from T_b to the lambda curve. An example is the isobaric temperature excursion.

For a constant depth of immersion in near-saturated He II the limiting ΔT-function increases monotonically as the system pressure (and with it T_b) is lowered . The resulting set of q_p-functions for various constant submersion depths is quite sensitive to the hydrostatic pressure difference created by the submersion. This sensitivity disappears in a pronounced way when the local pressure at the sample exceeds the pressure of the lower He^4 triple point (lambda point of saturated He^4 with coexistence of He II- He I and vapor). Above the triple point pressure the q_p-values depend on the difference $(T_\lambda - T_b)$. As $(T_\lambda - T_b)$ is raised, q_p rises first steeply. At low temperatures q_p saturates , and a change in $(T_\lambda - T_b)$ does not cause a significant variation in q_p .

Figure IV.6 indicates at temperatures $T_b < T_\lambda$ the drastic submersion depth effect for two values of this depth H , as predicted by the Soloski equation. Further details of single specimens are discussed subsequently in the context of insulating coatings and other effects.

Coating Influence. In the first part of this section the effects of insulating coatings on the quench onset will be discussed. In the subsequent second portion of this section we deal with various phenomena

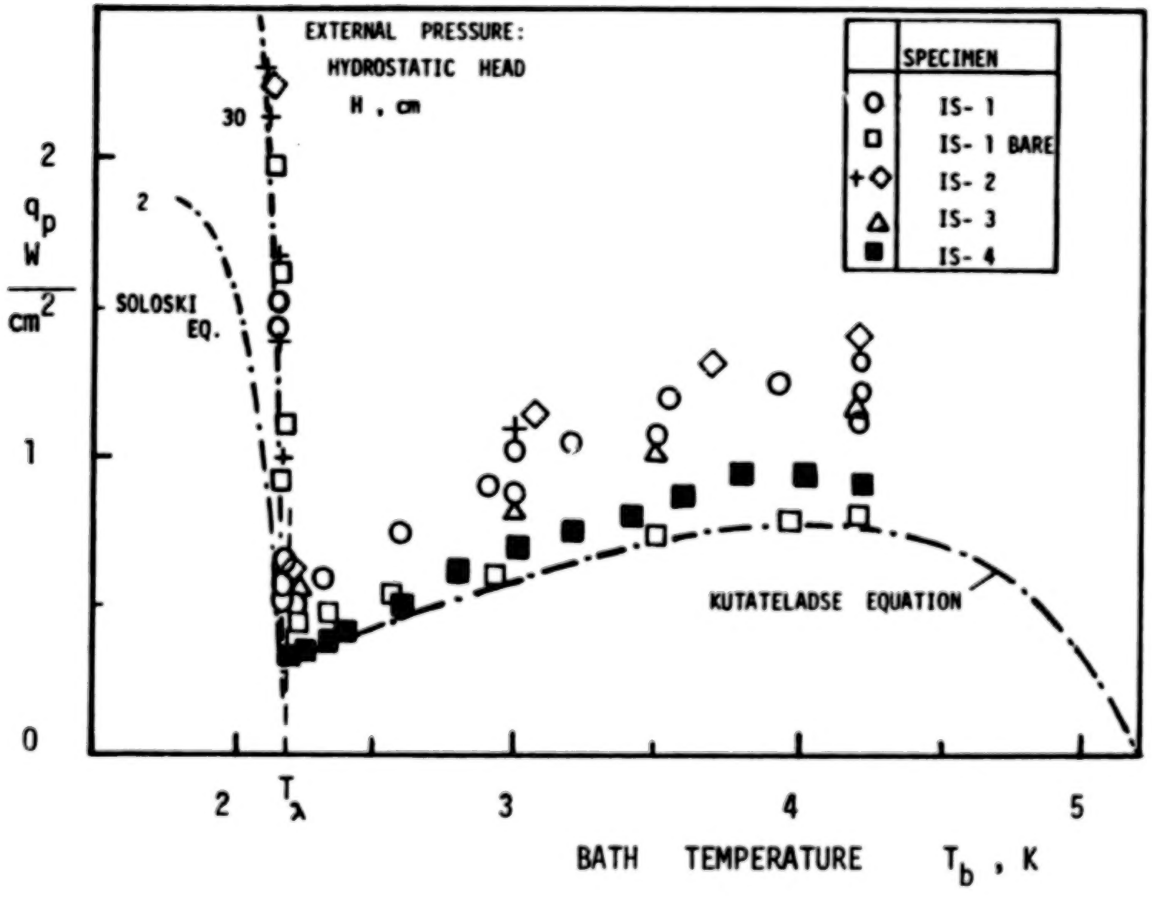

Figure IV.6. Peak heat flux density q_p of single specimens in near-saturated liquid^p

related to voltage-heater currents records for the pre-quench and post-quench regimes.

Simplified quench onset functions are introduced in Figure IV.7 in order to illustrate the coating influence. This figure contains the data of specimen IS-4 with formvar coating, and two other quench onset functions, $(q_o)_{Limit}$ and $(q_o)_{cu}$. The latter are based on a constant thermal conductivity k_i. The limiting function $(q_o)_{Limit}$ presumes existence of an insulator of thickness $d_i = 6$ μm with a thermal conductivity $k_i = 10^{-4}$ W cm^{-1} K^{-1}, i.e. of the same order as the formvar function k_{FV}. For this case we have $q_o = q_p$ at a certain T_b, namely 3.5K. Equality of the peak flux and the quench onset flux leads to the "limiting insulator thickness" δ_L which had been evaluated previously in Reference 1. Thus, post-quench regime B is eliminated for the thermodynamic state under consideration.

The other theoretical function is based on the presumption of a very thin coating thickness (e.g. minute oxide layer with negligible thermal resistance). Now it is assumed that damaged Cu in radial direction provides the dominant resistance with $k_{cu} = 1$ W cm^{-1}K^{-1}. The q_o-values of this case become quite large, and it is noted that this function is not meaningful for the present heater simulation technique. Instead, the peak heat flux density of the fluid phase transition phenomenon is the controlling factor. In the quench of a "bare" magnet, caused for instance by mechanical friction, a large range of undefined conditions exists between the quasi-steady functions q_o and q_p. (The latter is a transient quantity for rapid quenches). Therefore, from the point of view of built-in, passive safety, the thin oxide coating ($d_i << \delta_L$) is a highly unstable component of the magnet system. It is concluded that defined conditions are preferable, in particular optimized insulating coatings for improved quench and post-quench conditions.

We consider now some details of quench records. Records of the coated specimen IS-4 are presented as X-Y-plotter traces in Figures IV.8 to IV.11. They display the potential difference across the composite versus the heater current passing through the non-inductively wound

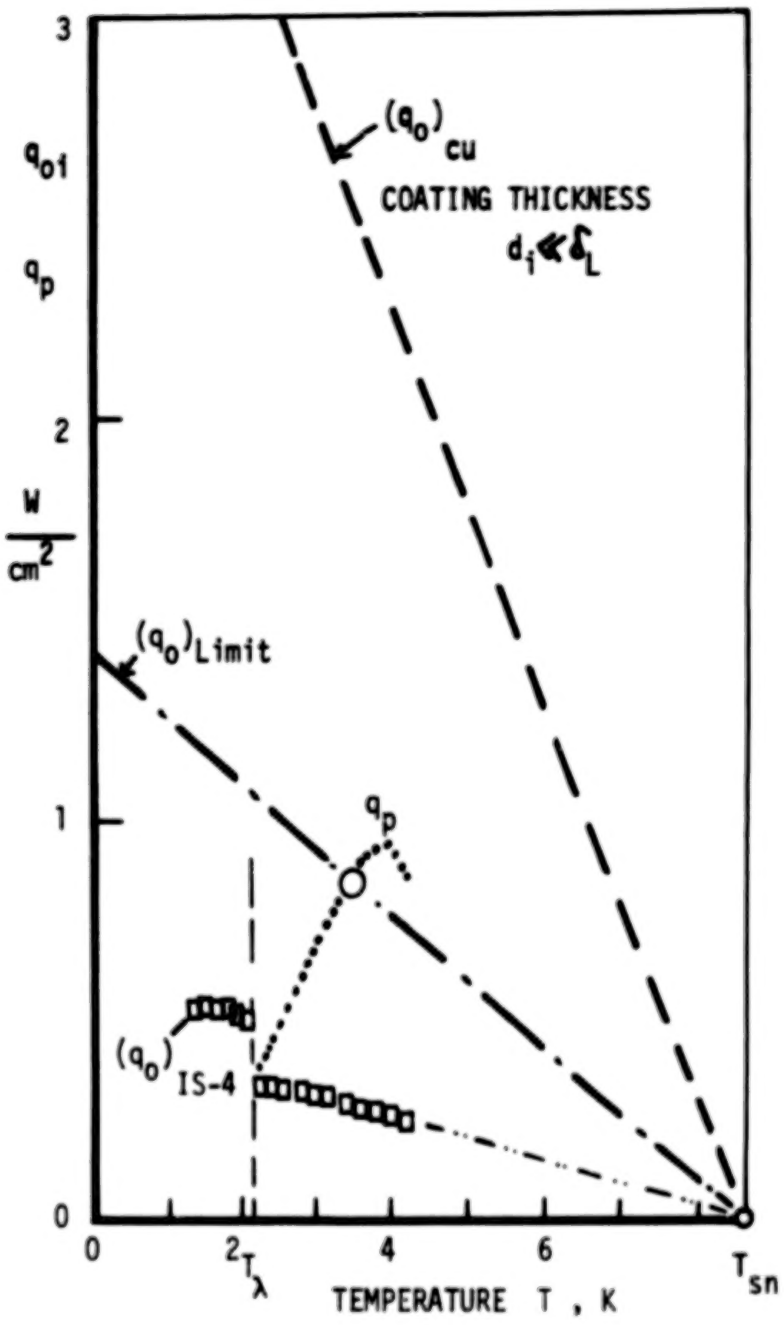

Figure IV.7 . Simplified quench onset functions q_{oi} and peak function q_p of IS-4;
$(q_o)_{IS-4}$ Data of specimen IS-4;

heater inside the specimen. Similar records of the uncoated specimen IS-5 are presented in Figures IV.17a to d. After the runs with these specimens the formvar coating of IS-4 was removed partially. Only the formvar on vertical faces was taken away initially (sample designation IS-4SB) in order to see possible modifications of the quench and post-quench behavior. Finally, the entire formvar coating was removed from the specimen (designation IS-4B). X-Y-plotter results are presented as Figures IV.13 to IV.16.

Referencing again the data for the single specimen IS-4 with formvar coating, we note several regimes which characterize the quench history. Destruction of the superconducting state of zero potential difference is initiated at quench onset. The latter is marked in Figure IV.8 for 4.2 K, as q reaches q_o at this appearance of detectable resistance. The onset point is most likely associated with a local transition of only a few of the type II filaments. There is a gradual transition to the normal state. The latter appears to be reached entirely when the potential difference indicates a "plateau" with rather minor changes in the voltage. This range is expected to correspond to temperatures from T_{sn} to about 25K. Above 25K the copper of the composite is useful as resistance thermometer. This is made possible by the large electrical resistance of the type II filament system in the normal state. Therefore, the current flows nearly entirely in the Cu. The latter has a residual resistance R_o small enough to permit noticeable changes in the entire resistance of the copper (R_{cu}). According to Matthiessen's rule, R_{cu} is the sum of R_o and the ideal resistance $R_{id}(T)$ associated with electron-phonon scattering. As the temperature is raised in post-quench regime B, some fluctuations on the record are interpreted as consequences of the onset of nucleate boiling. This range of fluctuations is followed by a rather flat region which is the result of efficient nucleate cooling. Finally, another "take-off" occurs at the peak flux of nucleate boiling. The latter appears to be preceded by local gradual heating in a small q-range. This seems to indicate transition boiling on part of the sample

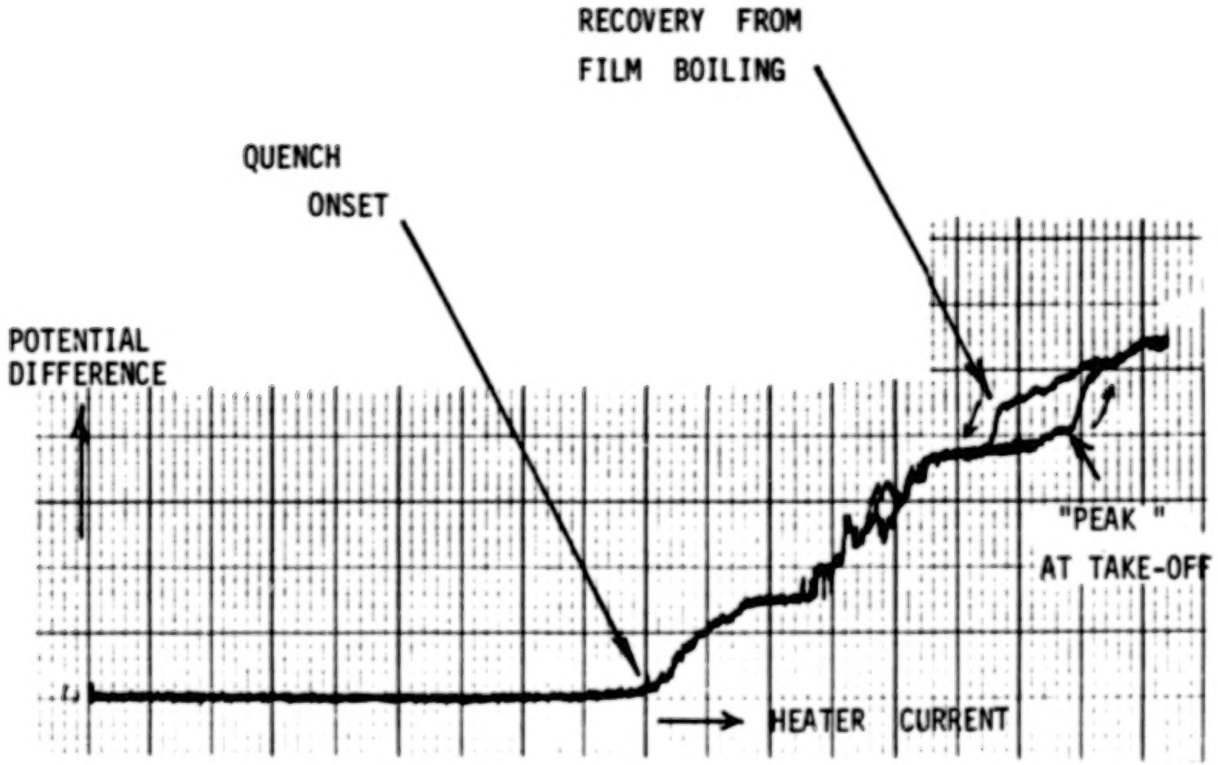

Figure IV.8 . Voltage versus heater current (arbitr. units) of the single, formvar-coated specimen IS-4; T_b = 4.2 K

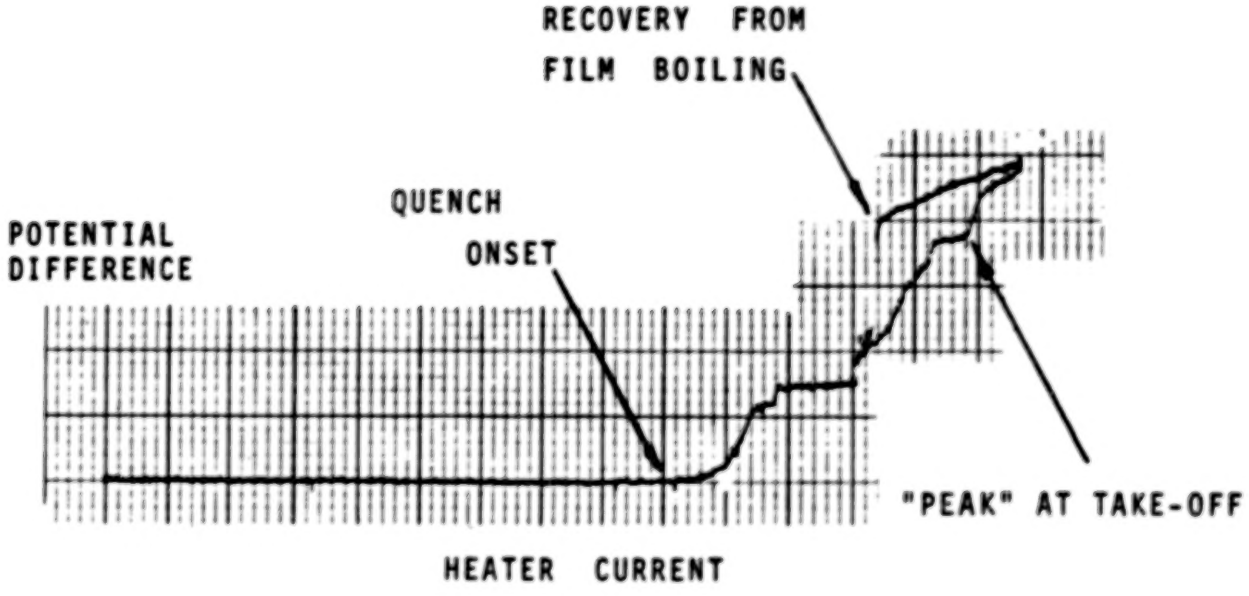

Figure IV.9 . Voltage versus heater current (arbitr. units) of the single , formvar-coated specimen IS-4 ; T_b = 3.0 K

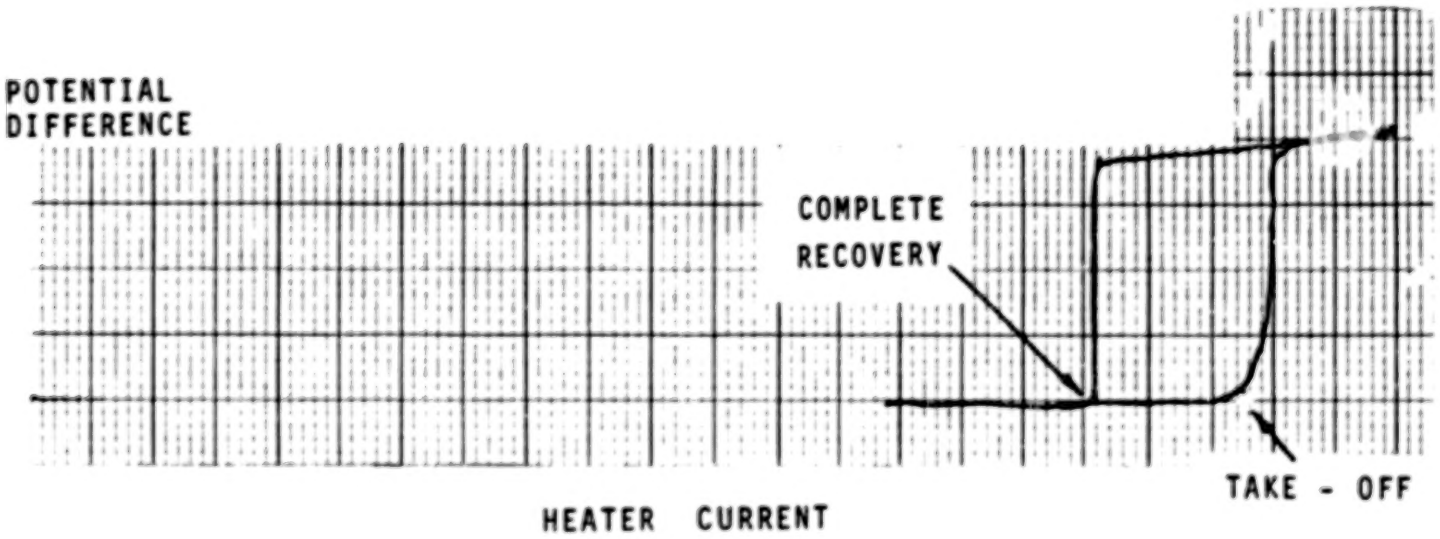

Figure IV.10. Voltage versus heater current (arbitr. units) of the single, formvar-coated specimen IS-4; T_b =2.2 K

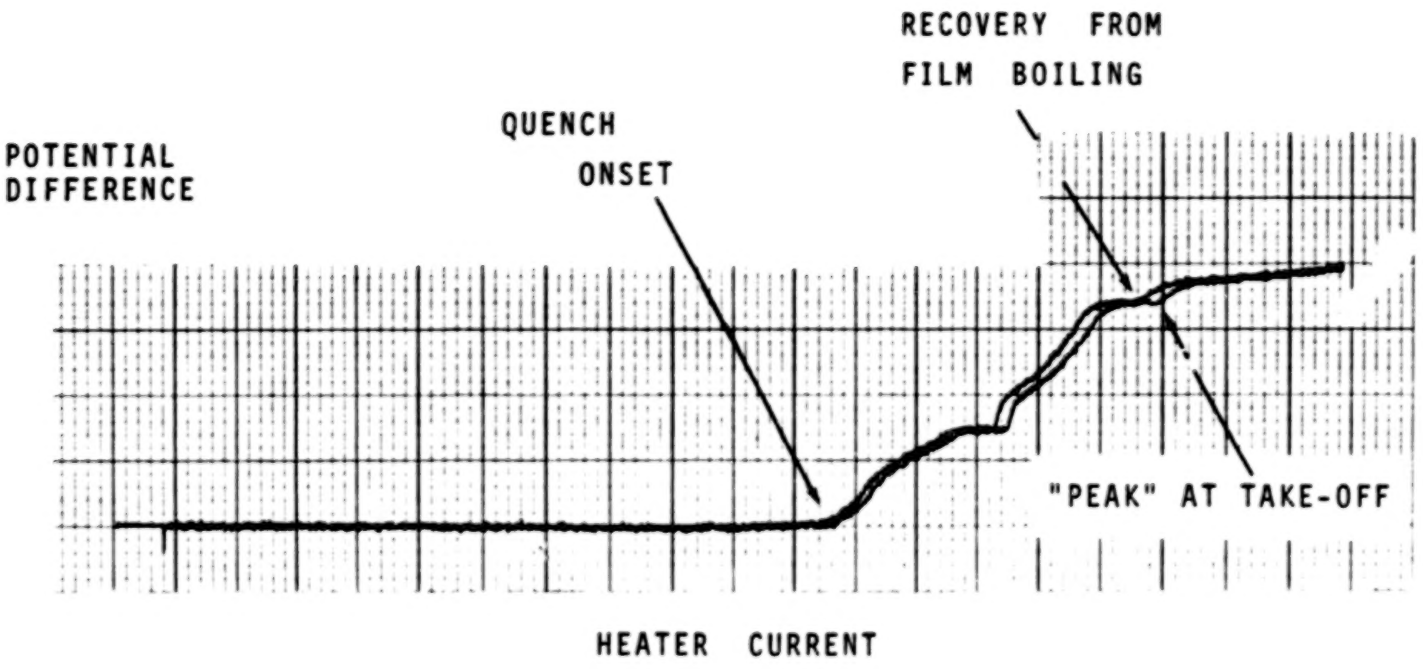

Figure IV.11. Voltage versus heater current (arbitr. units) of the single -formvar-coated specimen IS-4 ; T_b = 2.146 K

surface. After the transition to film boiling (at high R_{cu}), the post-quench regime C is established with rather inefficient cooling conditions. Upon power reversal ($dq < 0$) the system recovers from film boiling at a heater current below the take-off value. Subsequently, nucleate cooling in post-quench regime B can act again over a limited q-interval. The subsequent cooldown follows quite closely the previous curve for $dq > 0$, however the fluctuations are not reproduced exactly. Finally upon further decrease of q the superconducting state is recovered.

Figure IV.9 for a bath temperature of 3.0 K displays features similar to the record for 1 bar. However as He I is cooled down further toward the lambda transition, the limiting thickness comes close to the formvar thickness. At 2.2 K, Figure IV.10 shows quench onset and take-off currents rather close together. Post-quench regime B is eliminated for practical purposes. This has the consequence that the temperature excursion is quite drastic. The recovery current is considerably lower than the quench onset current. Therefore, a wide hysteresis loop is enclosed by the quasi-steady change of state.

Figure IV.11 pertains to He II. Now the limiting thickness has been reduced again to smaller values below the formvar thickness. There exists a broad range of q-values in post-quench regime B. Efficient cooling takes place as long as the Kapitza conductance between formvar and He II is large. Only a small film boiling loop shows up in the record.

Let us now examine specimen IS-4SB with bare Cu side walls exposed directly to the liquid. Figure IV.12 for the semi-bare sample contains qualitatively different phenomena. In particular we note that the film boiling hysteresis loop appears to be absent. At the bare surfaces film boiling may be established immediately after local quench initiation. In this region the Cu-thermometer is insensitive. Therefore, the record does not allow an assessment of this phase of the post-quench history. Aside from the hysteresis associated with quench onset and recovery of

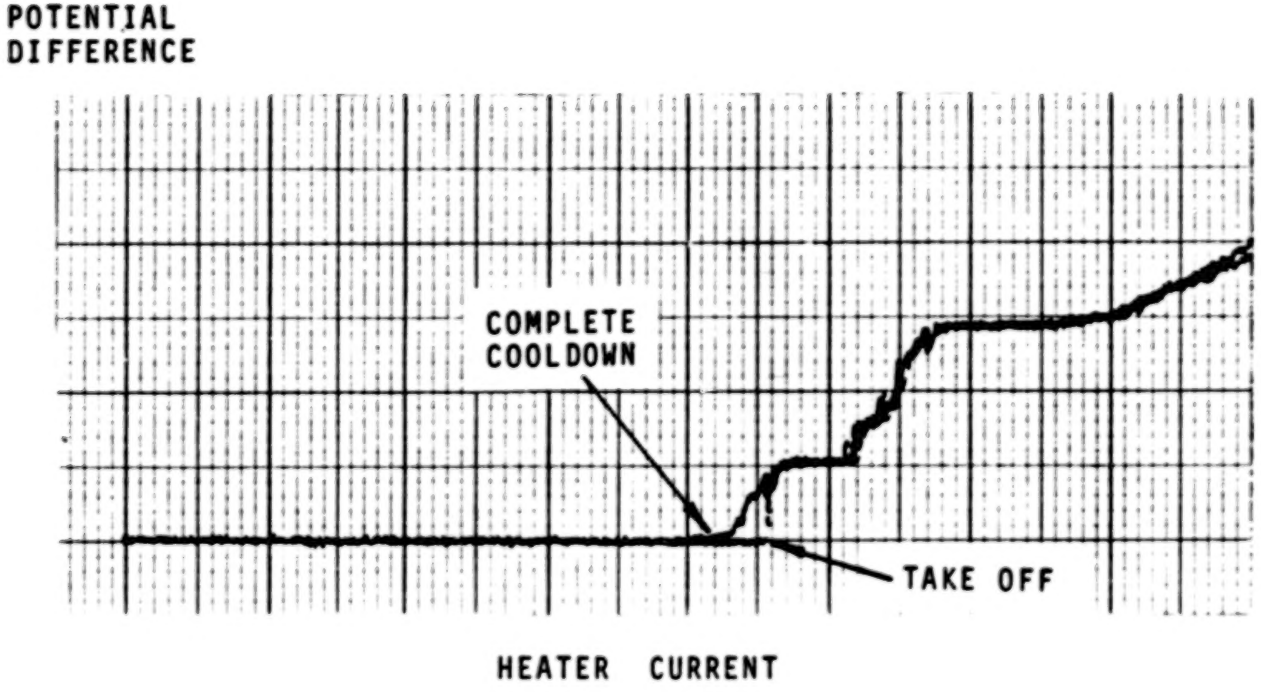

Figure IV.12. Voltage versus heater current (arbitr. units) of semi-bare specimen IS-4SB ; T_b = 4.2 K

superconductivity, no significant differences between the cases $dq > 0$ and $dq < 0$ seem to exist. It is concluded that bare surfaces of small size may produce local "hot" spots without serious effects on the rest of the system. This type of scenario, however, can only be expected when the formvar thickness is below the limiting thickness for the thermodynamic state selected.

The bare sample IS-4B has a very minute (unknown) micro-thickness of the surface impurity layer. This layer thickness is very much smaller than the limiting thickness δ_L. Therefore, post-quench regime B is eliminated. At 4.2K, Figure IV.13 exhibits a rapid takeoff which terminates the superconducting state with a transition into the film boiling regime. After power reversal ($dq < 0$), an abrupt change in the derivative of the post-quench curve indicates cessation of film boiling conditions. There is another plateau interpreted as a q-range with efficient cooling in the temperature range $T_{sn} < T < 25$ K. Subsequently complete recovery from the normal state is indicated on the record. These features appear to be present in the various He I-runs with IS-4B (Figures IV.13 to IV.15). A departure from this behavior occurs in He II in so far as there is a post-quench range of oscillatory phenomena after the termination of film boiling. (Figure IV.16).

Sample IS-5B reproduces the major characteristic features of IS-4B. In Figure IV.17 d however, no excessive oscillations are seen at He II conditions of the bath. The fluctuation pattern of film boiling is quite pronounced. In this respect He I and He II appear to show similar features in post-quench regime C.

We turn now to an assessment of coating effects on q_p. According to the various quench records, several post-quench phenomena are possible which depend on a set of variables, such as the thermodynamic state and coating conditions. In addition, other factors have become known from boiling studies of liquids at temperatures of the order 10^2 K. One quantity is the micro-roughness of the surface (e.g.

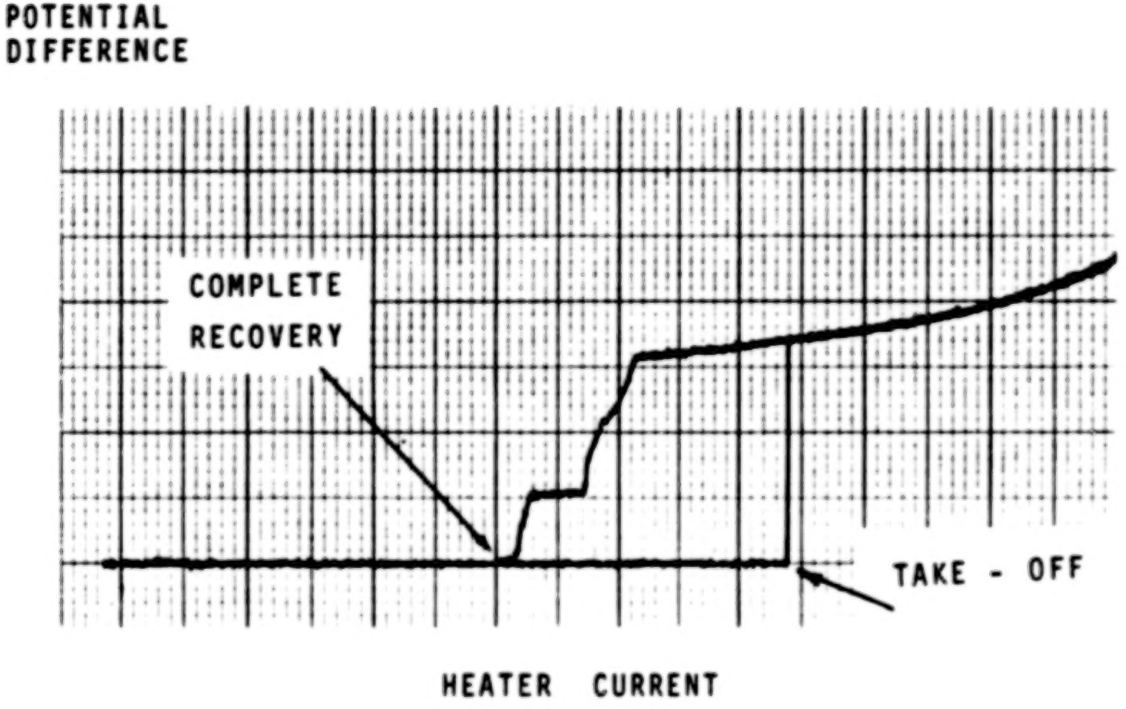

Figure IV.13. Voltage versus heater current (arbitr. units) of bare specimen IS-4B ; T_b = 4.2 K

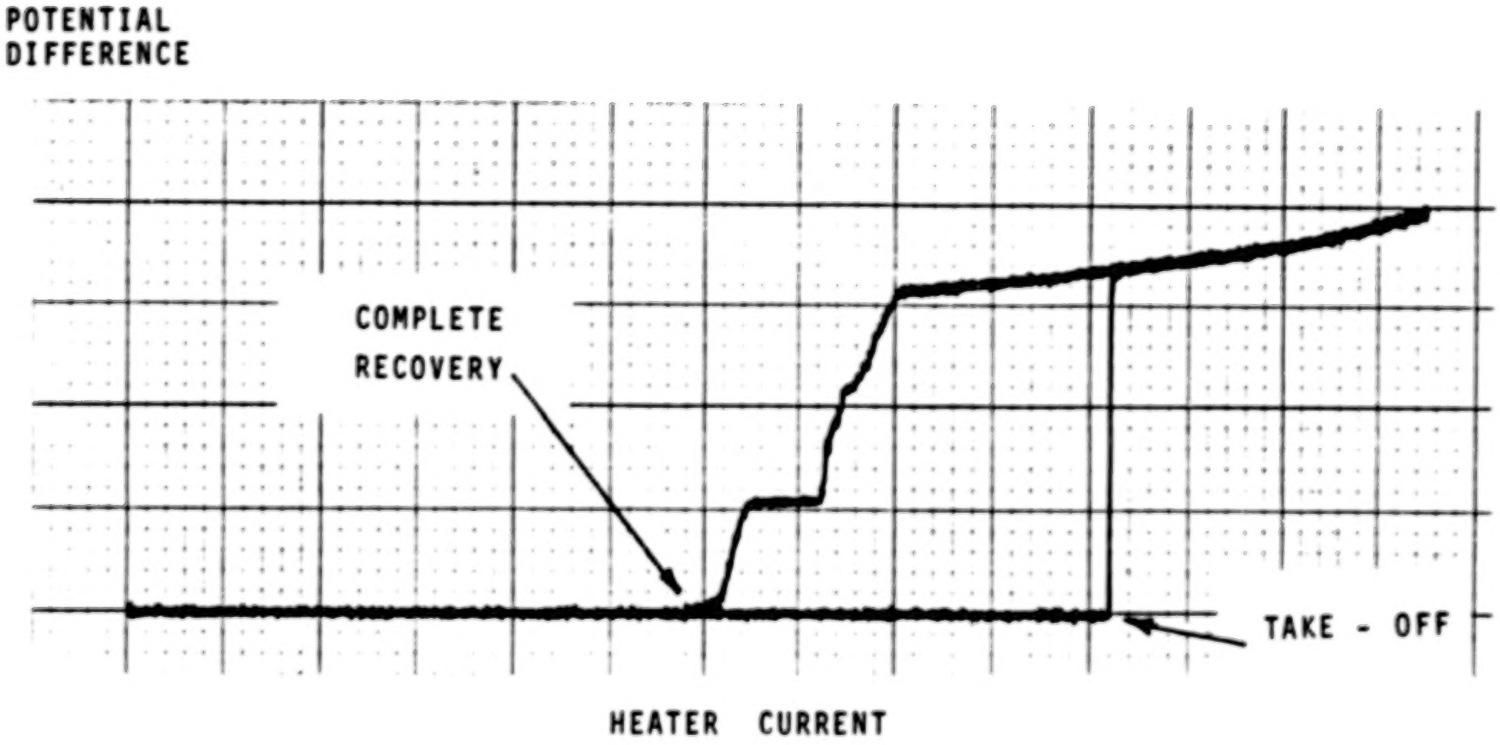

Figure IV.14. Voltage versus heater current (arbitr. units) of bare specimen IS-4B ; T_b = 3.0 K

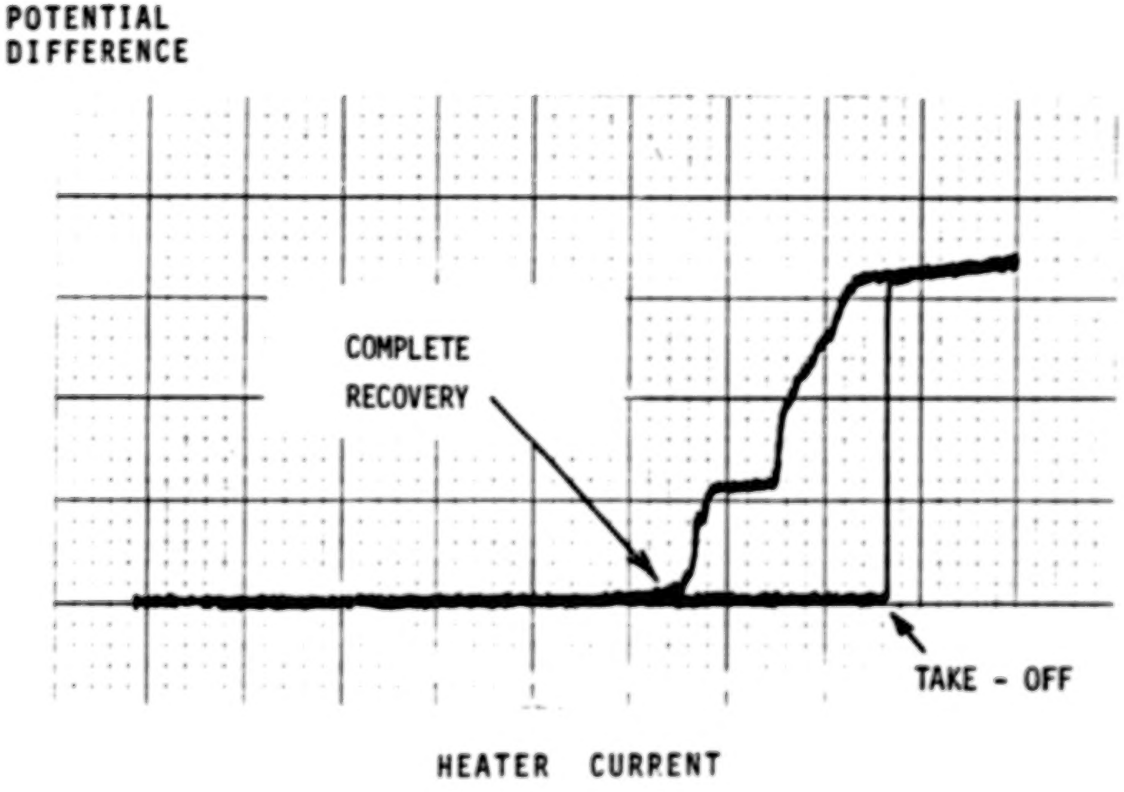

Figure IV.15. Voltage versus heater current (arbitr. units) of bare specimen IS-4B ; T_b = 2.2 K

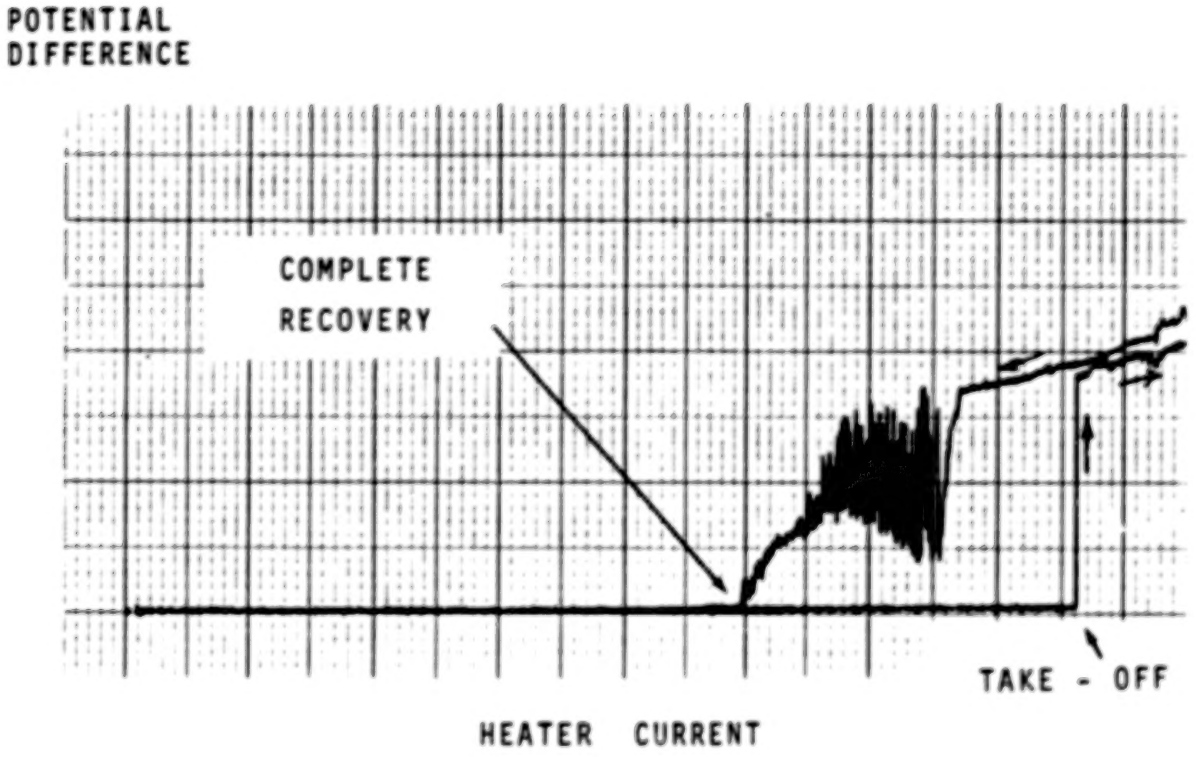

Figure IV.16. Voltage versus heater current (arbitr. units) of bare specimen IS-4B ; T_b = 2.15 K

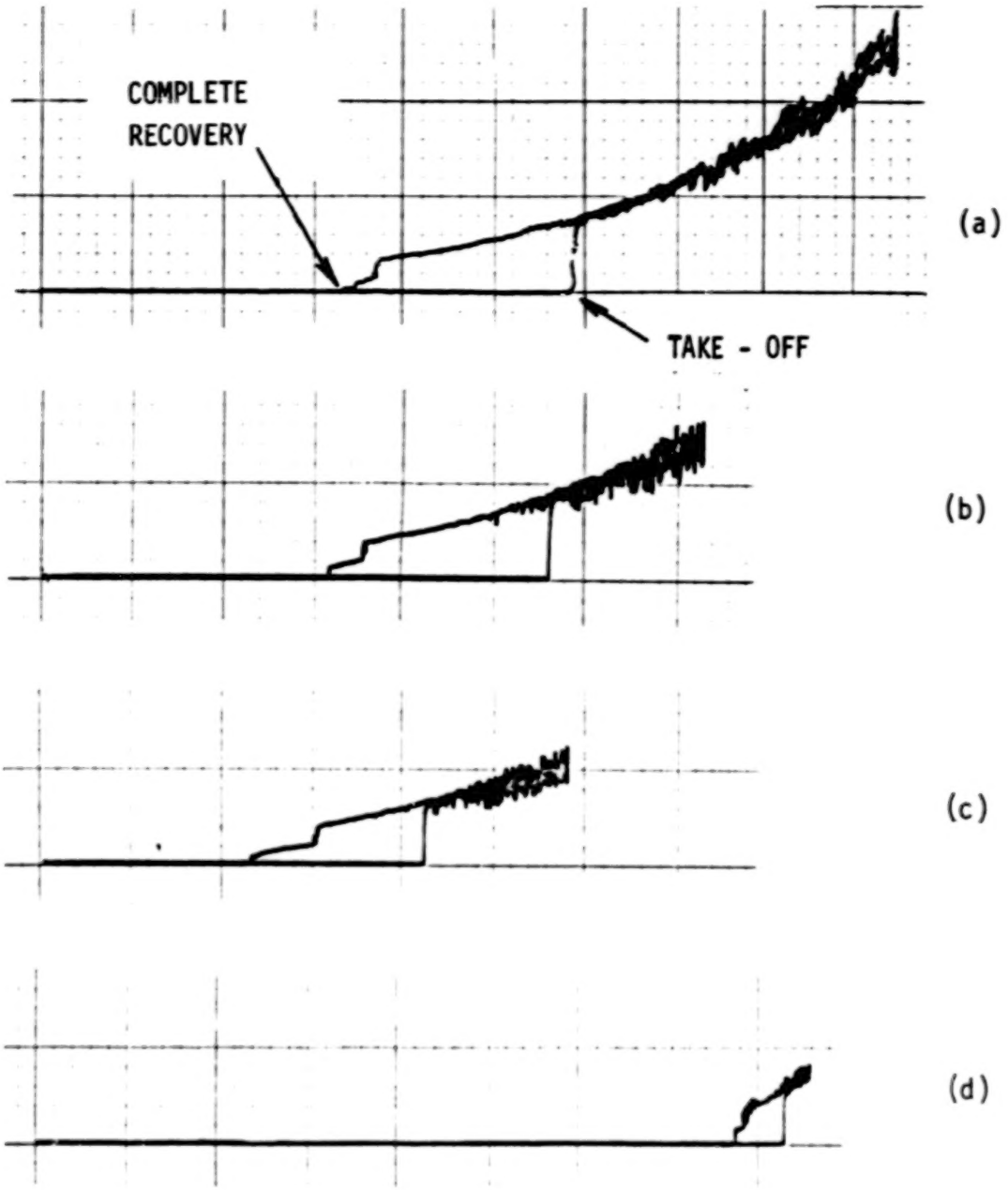

Figure IV.17. Potential difference in arbitrary units versus heater current (arb. units) of specimen IS-5 (bare);
a. Bath temperature T_b = 4.2 K ;
b. Bath temperature T_b = 3.0 K ;
c. Bath temperature T_b = 2.2 K ;
d. Bath temperature T_b = 2.15 K

Reference 12) . Another variable is the orientation , and a third one the size (e.g. diameter of horizontal cylinders with circular cross section).

As far as the influence of the microroughness is concerned, there appear to be no quantified documented details in the He I literature. It is noted that all other substances (aside from the He isotopes) are frozen. Therefore most cryotechnology surfaces appear to be "coated" with a minute layer of adsorbed molecules. These may be most likely air molecules (including "smoggy" air constituents). When special precautions are taken the composition may change toward higher He^4 concentrations resulting from purging with He^4 gas.

Concerning orientation effects we note that gravity forces have a distinct influence on two-phase motion in He I during boiling. According to Reference 13, a horizontal surface with heat flow up has the largest q_p . As the angle of inclination ϕ between the normal to the surface and the gravitational direction is varied, there is a monotonic decrease of q_p with increasing ϕ . As seen in Figure IV.18 , the rate of change of q_p with ϕ varies with the bath temperature. A first order approximation is insertion of the gravitational force component (and buoyancy force component respectively) in the Kutateladse equation :

$$q_p = 0.16\, \lambda \rho_v^{1/2} \left[\sigma (\rho_L - \rho_v) g \cos \phi \right]^{1/4} \qquad \text{(IV.12)}$$

(λ latent heat of vaporization , σ surface tension , g gravitational acceleration , ρ_L , ρ_v density of saturated liquid and vapor respectively) . In the limit $\phi \to 0$, the usual form of the Kutateladse equation is recovered (as shown in Figure IV. 6) . Figure IV.18 indicates that Equation IV.12 is quite useful at 4.2 K in the range $0 < \phi < \pi/4$. However at lower bath temperatures the range of validity appears to be restricted to a smaller ϕ- interval . When ϕ reaches $\pi/2$, q_p drops to about 2/3 of the value for $\phi = 0$ at $T_b = 4.21$ K . A qualitatively similar decrease of q_p was found also in the present runs when the sample orientation was changed from "diamond" position to "square" position.

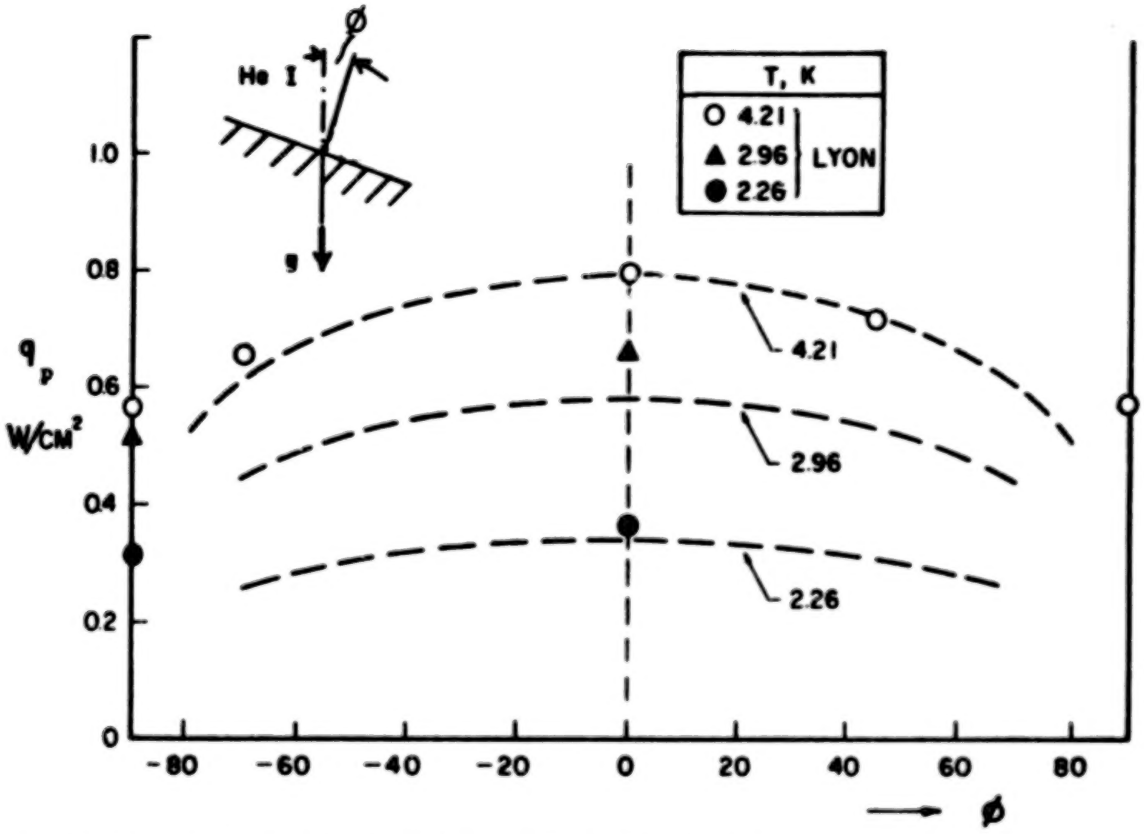

Figure IV.18 . Influence of surface orientation on q_p

As far as the influence of the size is concerned we note that recent transient experiments at 4.2 K report rather large q_p-values in the limit of quasi-steady transport (Reference 14). These data confirm in part early findings with normal metal wires. At slow transients (at $dq > 0$) improvements in q_p by about a factor of 2 were obtained under some conditions. However the degree of stratification of the bath appeared to exert some influence.

Reconsidering the present results we emphasize that the coating influence was quite distinct: The coated samples had persistently larger q_p-values than the uncoated samples. However, in view of the other factors discussed above we conclude that the enhancement of q_p due to coating is by far not as spectacular as other benefits derived from coating application.

"Fin Effects" Resulting From Conductor Length. The long single conductor in a pool permits a significant amount of longitudinal conduction compared to radial heat transport. In thermal experiments various techniques are used to keep heat leaks under control which may incorporate errors. For instance even with guard heaters and vacuum insulation there is a chance that nucleation of vapor may occur preferably at joint locations. These domains may have different nucleation agents with enhanced heat removal rates. Therefore, heat leaks into directions undesired are a possibility. Though some early tests aimed at technology results,which include the longitudinal thermal conduction in composite conductors, it appears to be useful to separate various heat transport contributions. Once a normal "hot" spot in the composite has been created, the longitudinal transport may be regarded as fin influence. This fin contribution is treated on the basis of simplified assumptions.

In a solenoid the conductor length is regarded as very long compared to the characteristic length of the fin L_F. It depends on both, radial and axial properties.

$$L_F = [(A_{cu}k_{cu})/(\bar{U}_1 C_c)]^{1/2} \qquad (IV.13)$$

($\overline{U_1}$ of Equation IV.1) . For an illustration we simplify $\overline{U_1}$ to $\overline{k_{FV}}/d_{FV}$ and a perfect square cross section ($C_c = 4a$) . Further A_{cu} is a fraction $(1 - \alpha)$ of the total cross section ; (α = ratio of type II to total cross section is about 3.7). For example , the ratio $(1-\alpha)a^2/4a$ is about 0.04 cm. For k_{cu} of the order 10 W $cm^{-1}K^{-1}$, a formvar value of $\overline{k_{FV}}$ of the order 10^{-4} W cm^{-1} K^{-1} , and $d_{FV} = 3 \cdot 10^{-3}$ cm, we obtain a characteristic fin length of the order $L_F \sim 3$ cm .

For these simplified assumptions we introduce a fin enhancement factor at quench onset ($\zeta_F > 1$). The radial heat transport is simplified to

$$Q_{rad} = L\, C_c (\overline{k_{FV}}/d_{FV})\, \Delta T_{sn} \qquad \text{(IV.14)}$$

(with ΔT_{sn} at quench onset). The longitudinal transport augmented by the fin contribution may be written as

$$Q_F = k_{cu}\, A_{cu}\, (\Delta T_{sn})/\, L_F \qquad \text{(IV.15)}$$

Consequently , the total rate of thermal transport at quench onset is expressed as

$$Q_{tot} = Q_{rad} + Q_F = Q_{rad}\, \zeta_F \qquad \text{(IV.16)}$$

with an enhancement factor

$$\zeta_F = 1 + (k_{cu}/\overline{k_{FV}})\, (d_{FV}/L_F)\, [(1-\alpha)\, 0.25\, a/L\,] \qquad \text{(IV.17)}$$

This factor is of the order of magnitude 2 for the length L of the present specimens . It is concluded that a significant portion of the thermal energy of the post-quench scenario is carried in longitudinal direction under suitable circumstances.

It cannot be expected that this large enhancement factor pertains to all cases (in particular high magnetic fields).Further, in general the enhancement at quench onset will not be the same at q_p . However, a first order approximation for post-quench regime B may be the

assumption that the enhancement factor does not change drastically for a specified bath condition. This would imply that both, q_o and q_p, are raised in roughly the same manner. Comparing the coated composite with uncoated conductors we note that a much smaller L_F-value will result when other variables are kept constant.

Figure IV.19 plots the factor $(\zeta_F - 1)$ versus bath temperature for near-saturated He^4. In He II a smaller enhancement results from the good radial transport and related shortening of the fin length. In He I there exists a flat minimum. When the limiting thickness is reached ζ_F becomes larger near T_λ. However this should not be interpreted as an attractive choice because of the elimination of post-quench regime B.

According to these studies of quasi-steady quench phenomena and post-quench scenarios, the coated composite conductor provides a minor increase in q_p. In addition however considerable benefit is obtained when the coating is "taylored" to include a sufficiently broad regime B. This will produce beneficial post-quench cooling conditions, and a satisfactory enhancement of thermal transport by longitudinal conduction. No quantitative design basis however will be obtained without a detailed check of the actual winding configuration, and conductor spacing with cooling possibilities respectively. Therefore we turn to the investigations of the composite conductor bundle.

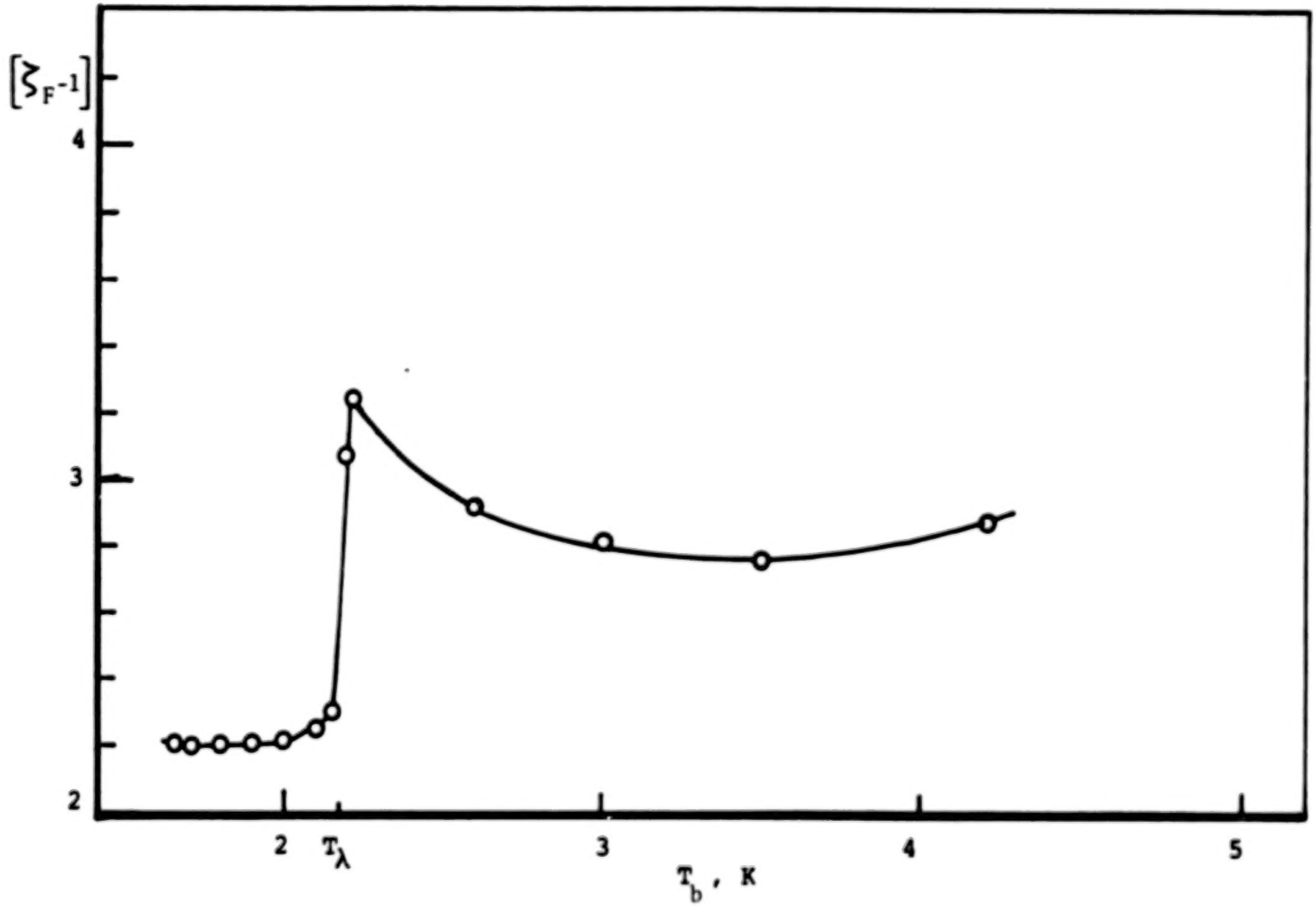

Figure IV. 19 . Fin influence versus saturated bath temperature;(Specimen IS-3B)

V. QUENCH ONSET OF THE CONDUCTOR BUNDLE AND RELATED QUENCH PHENOMENA

Figure V.1 permits a comparison of the runs for two different duct orientations. These data for quench onset show the largest variation of the thermal conductance $\overline{U_{oB}}$ (per diathermic area) when the duct-spacer system is arranged in horizontal direction. In contrast, the vertical duct - spacer system appears to permit action of buoyancy forces on the vapor phase without large flow impedances at 4. 2 K. At this temperature the vapor bubbles appear to be quite small compared to the spacer thickness. As the pressure is reduced more and more toward the lambda transition pressure of saturated liquid, the bubbles become larger and larger. Therefore, it appears probable that interference between vapor and duct walls causes a complicated liquid-vapor two-phase motion (flow boiling) . In the horizontal duct gravitational buoyancy cannot act directly. Therefore , viscous and turbulent fluid-wall interaction is expected to produce flow conditions dependent on the duct length. This leads to the lowest $\overline{U_{oB}}$-value . Near the critical point the vapor bubble size becomes very small, and disappears , as the pressure P approaches P_c , the critical pressure. Therefore, again small $\overline{U_{oB}}$ -values result. In He II the Kapitza layer impeding thermal transport on the fluid side of the "solid-liquid junction" is quite thin,i.e. very much smaller than the duct width. Therefore, no differences between horizontal and vertical ducts are observed (within data scatter). Compared to the thermal conductances of single specimens at quench onset, there appears to be a larger variation in $\overline{U_{oB}}$ with pressure and temperature respectively. To permit a closer inspection we introduce a simplified thermal circuit which expresses bundle resistances in terms of single specimen contributions.

Thermal Circuit. A simplified thermal circuit is adopted for quasi-steady flow, as sketched in Figure V.2 a and V.2 b The bundle is considered two-dimensional . Figure V.2 a is a schematic of the geometry with two heat current contributions (Q_1 and Q_2). Contribution Q_1 passes

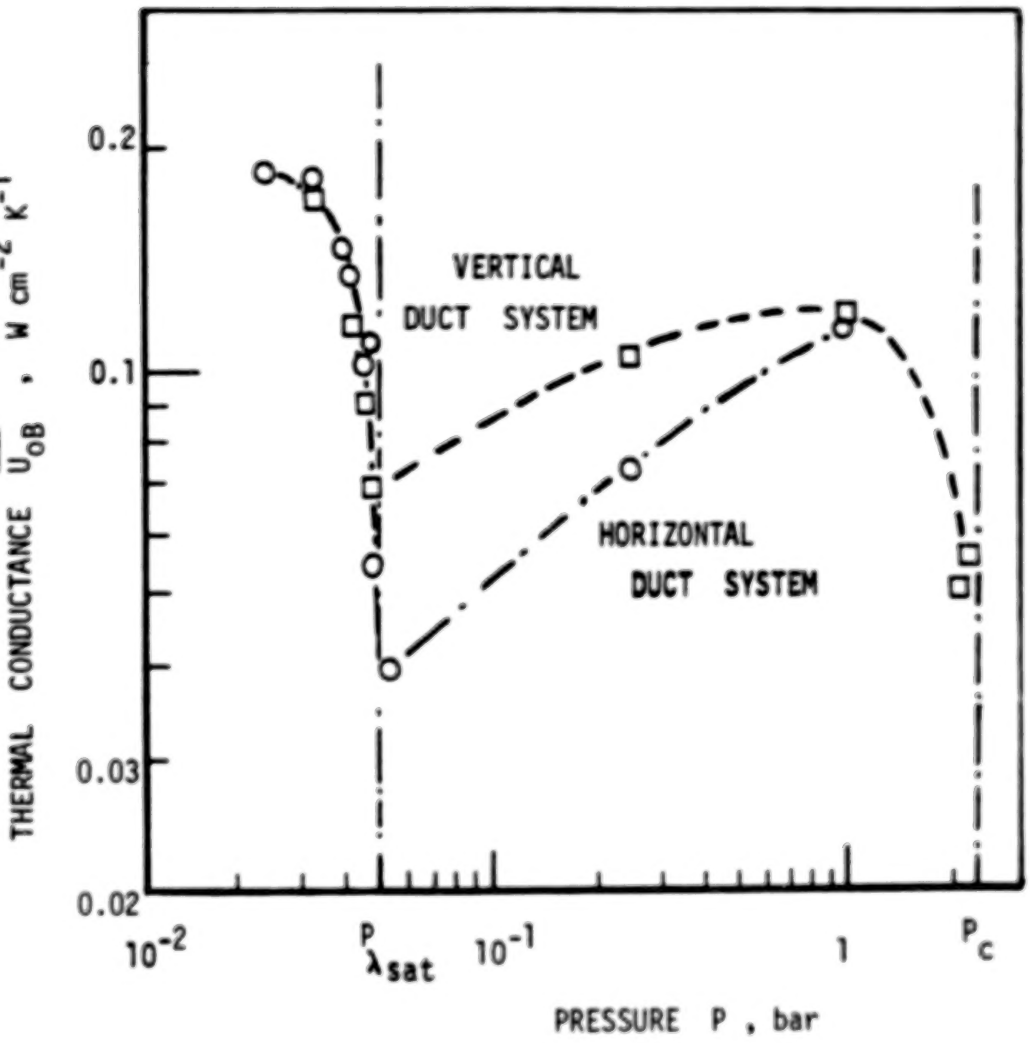

Figure V.1 . Overall thermal conductance of conductor bundle at quench onset for two different orientations of the spacer-duct system

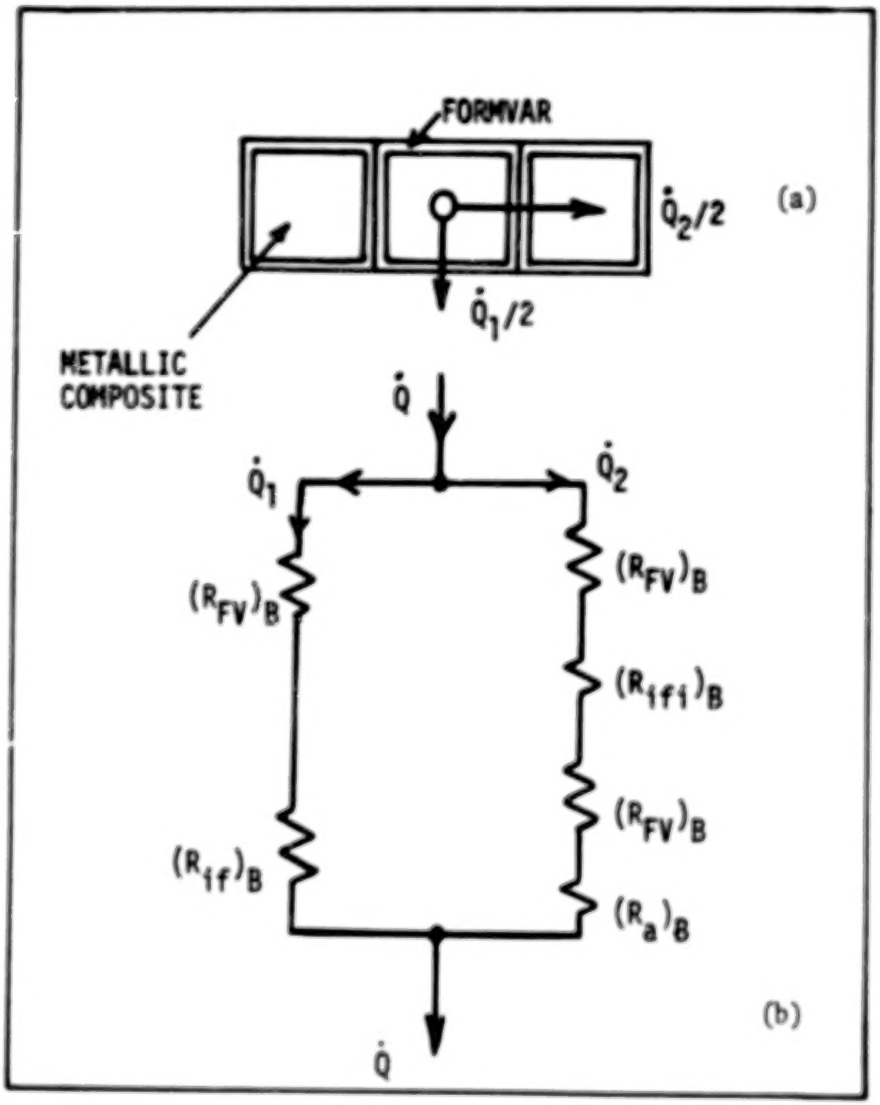

Figure V.2 . Simplified thermal circuit for conductor bundle ; (a) Configuration; (b) Circuit

directly from the central (energized) conductor to the fluid. Therefore the impedances should be similar as long as the solid-fluid interaction does not change . Contribution Q_2 is transported first from the central conductor CB to the adjacent conductors . (Only $Q_2/2$ is shown in the Figure V.2 a). Subsequently, solid conduction takes place with a final transfer of Q_2 to the fluid.

For path 1 of Q_1 , Figure V.2 b indicates two dominant thermal resistances: The formvar layer resistance $(R_{FV})_B$ and the resistance resulting from solid-fluid interaction [$(R_{if})_B$] . For simplification it is assumed that each of the 2 resistances is equal to the single specimen value . Path 2 for Q_2 has two formvar layer resistances and a contribution from a fluid layer in between . The latter resistance designated as $(R_{ifi})_B$ would not arise if the conductor surfaces would be perfect planes in close contact with each other. However because of geometry imperfections some fluid will be in between the conductors . Finally, all other additional resistances are summarized as $(R_a)_B$. It appears that this circuit is quite complicated with non-linear contributions from solid-fluid interaction terms. Along the line of previous circuit simplifications (Figure IV.3 for the single specimen) we proceed to a rather simple limit which involves only the formvar layers and related areas. This circuit is sketched in Figure V.3 .

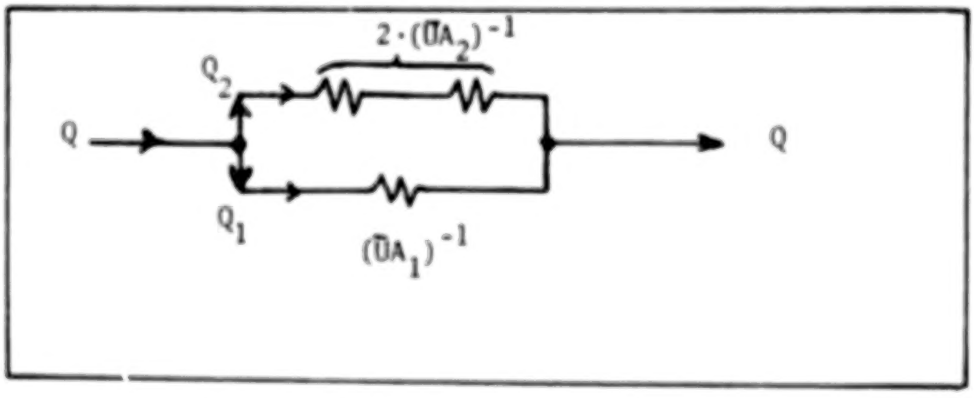

Figure V.3 . Simplified bundle circuit of thermal resistances

Figure V.3 incorporates only contributions of the single specimen $\overline{U} = U_1 = k_{FV}/d_{FV}$. The area A_1 of path 1 is expressed in terms of the total area A_{tot} using the area ratio $f_A = A_1/A_{tot}$; ($A_2 = [1 - f_A] A_{tot}$). The resulting conductance of the bundle is

$$\overline{U_B} = \overline{U_1} [f_A + (1 - f_A) / 2]$$
$$= \overline{U_1} \cdot (1 + f_A)/2 \qquad (V.1)$$

These conditions are considered for the special point $q = q_o$ on the quench characteristics , i.e. quench onset designated by the subscript o.

$$\overline{U_{oB}} = \overline{U_{o1}} (1 + f_A)/2 \qquad (V.2)$$

The limiting case $f_A \rightarrow 1$ correponds to the conductance of the single specimen : $\overline{U_{oB}} \rightarrow \overline{U_{o1}}$. For a perfect square cross section with $A_1 = A_2 = A_{tot}/2$, or a factor $f_A = 1/2$, we obtain a ratio $\overline{U_{oB}}/\overline{U_{o1}} = 0.75$. Slightly higher values of this ratio are found for the real area ratio f_A of about 2/3 . Accordingly, a slight decrease of $\overline{U_{oB}}$ is predicted by Equation (V.2) with respect to the single sample value $\overline{U_{o1}}$.

The bundle data of the present experiments appear to be in partial agreement with prediction of the simplified model . Figure V.4 plots conductance ratios of the horizontal duct system and includes Equation (V.2) for various area ratios f_A . There is no severe order of magnitude reduction of the thermal conductance at quench onset. The temperature dependence however is more pronounced . This is seen in particular when T_b is lowered in He I toward the lambda transition . The results are interpreted as evidence for worsened solid-coolant interaction due to enlarged fluid flow impedances. The latter are most likely a consequence of the larger vapor bubble size at low T_b . In He II again a pronounced rise of $\overline{U_{oB}}$ is the result of additional effects associated with the bundle specimen , in part departures from the assumption of two-dimensional flow conditions . The reference conductance used in Figure V.4 is the set of data of the individual specimen IS-1. For

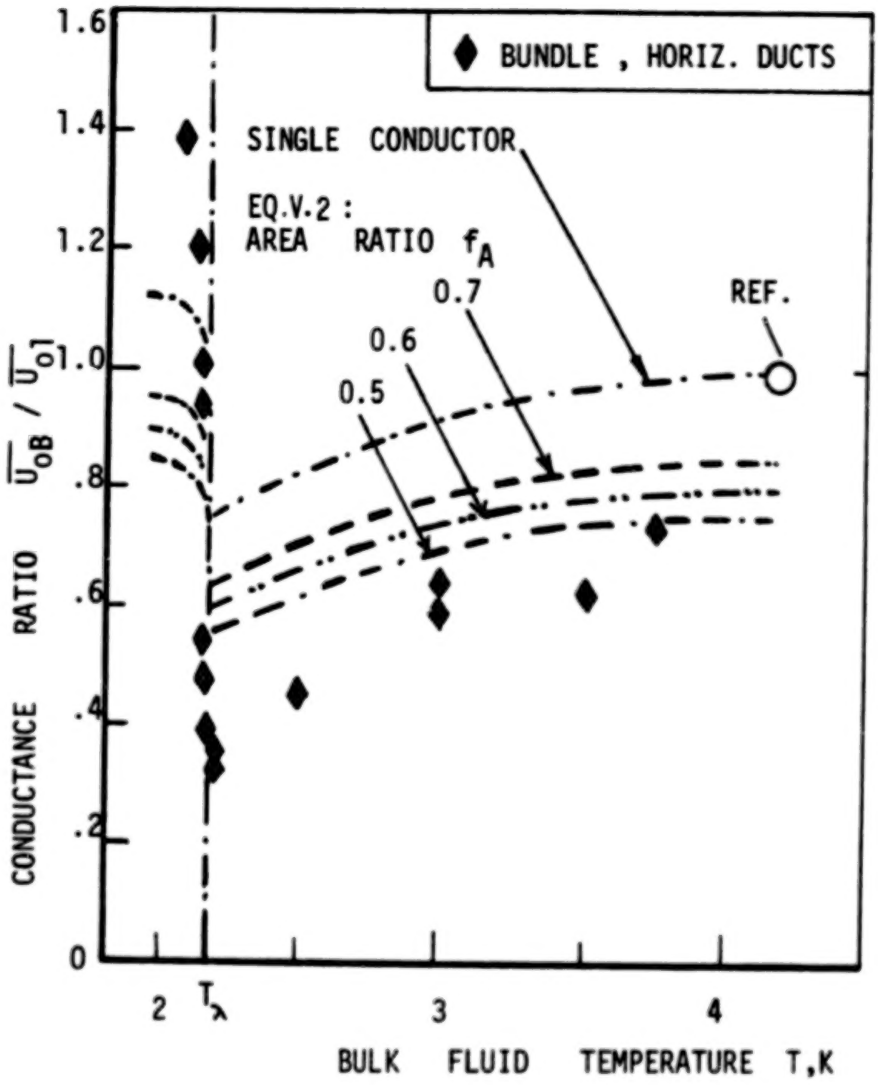

Figure V.4. Conductance ratio of bundle with horizontal duct system;
Reference : Single specimen IS-1

further elucidation of a possible reduction of U_B , and q respectively, we consider subsequently the bath temperature influence $q(T_b)$ of near-saturated liquid He I.

For single specimens with vapor removal by gravitational buoyancy the Kutateladse equation predicts the T_b-influence when the bubble size is a significant parameter. Now we turn to the coolant confined by a narrow duct whose size is the dominant dimension ,i.e. the vapor bubble size is too large or comparable to the order of magnitude of the duct size. The last point of post-quench regime B is q_p. For this q-value one of the simplest phenomenological equations describing vapor removal appears to be the Sydoriak-Roberts equation (References 15 and 16). The truncated version of q_p may be rewritten as heat flux density W_p per duct cross section

$$W_p = K_{SD} \lambda (\rho_v \rho x_e \tilde{H} g)^{1/2} \qquad (V.3)$$

(duct axis vertical; K_{SD} = constant , x_e quality at exit of duct , $\tilde{H}$ height of heated duct , and effective duct length respectively, effective density $\rho = [x_e/\rho_v + (1-x_e)/\rho_L]^{-1}$) . The exit vapor quality has been determined as $x_e \approx 0.3$. Further, the constant K_{SD} may vary from one geometry to the next, in particular when the heated length is varied with respect to the overall length of the duct. Usually the magnet ducts are open on top and at the bottom. However even for geometries with a closed lower end , an open upper end , and a localized wire heater inside the insulated duct, Equation (V.3) appears to predict the W_p-values reasonably as far as the T_b-dependence is concerned. An example is the arrangement used in Reference 17 . It is characterized by the constant $K_{SD} = 7.3\ 10^{-3}$. Therefore, a comparison of the T_b- influence of one and the same fluid ,i.e. He I, on q_p and on W_p appears to be meaningful.

Figure V.5 displays the peak flux functions normalized in terms of their maximum values q_{pmax} and W_{pmax} . The evaluation has been based upon simplified thermodynamic functions expressed in terms of critical quantities (T_c critical temperature , ρ_c critical density).

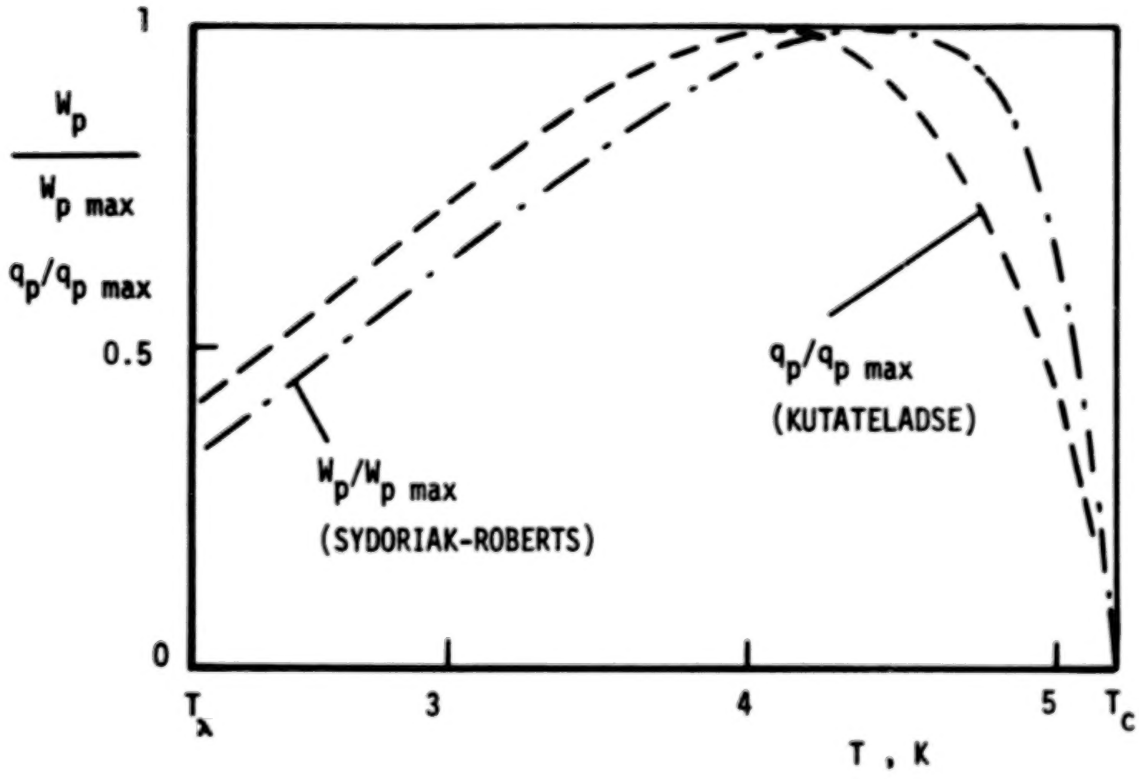

Figure V. 5 . Heat flux density ratios of vapor removal equations ;
(Subscript max = maximum value)

The functions utilized are:

Density difference (Reference 18):

$$(\rho_L - \rho_v)/\rho_c = 3.5\,(1 - T/T_c)^{1/3} \qquad (V.4)$$

Density ratio (Reference 18) :

$$\rho_v/\rho_c = 1 + 0.75\,(1 - T/T_c) - 2.25\,(1 - T/T_c)^{1/3} \qquad (V.5)$$

Latent heat (Reference 19) :

$$M^{5/4}\,(\rho - \rho_v)^{-1} = \text{const} \qquad (V.6)$$

Surface tension (Reference 20) :

$$\sigma = [\,M/(\rho_L - \rho_v)\,] = P_{SP} \qquad (V.7)$$

(M = molecular mass ; σ surface tension ; P_{SP} two-phase equilibrium parameter). Though more complex functions have become known for the various thermophysical properties (e.g. Reference 21 for σ), we note in Figure V.5 rather close qualitative agreement in the T_b-aspects. There exists a maximum in both cases, and a decrease toward zero at the thermodynamic critical point. Toward the lambda point limit the two functions retain values not too far below 0.5 . There is a shift in the temperature of the maximum, however a most important influence of the product ($\lambda\,\rho_v$) appears to be common to both cases . In other words, the effective velocity $q_p/(\rho_v \lambda)$, and $W_p/(\rho_v \lambda)$ does not appear to undergo drastic order of magnitude changes. Therefore we expect for other magnet ducts a similar reduction of q-values in He I below 3 K and above 4 K . The geometry of the spacer duct system may produce important changes of K_{SD} , and details of viscous two-phase flow in flow boiling systems have been described in the literature (e.g. Reference 22). Nevertheless , we remark that , aside from Reference 16 other heater simulation studies confirmed the duct size effect predicted by Equation V.3 . Experimental results for plane channels have been reported in Reference 23 and data for small solenoids with vertical axis in Reference 24. Related stability conditions of normal zone evolution at 4.2 K are the subject of a recent paper (Reference 25).

VI . COOLDOWN OF COMPOSITE CONDUCTORS FROM POST - QUENCH CONDITIONS

Cooldown experiments from either post-quench regime B or from regime C were conducted with formvar-coated and bare specimens,and with the bundle . Initially the system was energized to a heater current value I_i corresponding to the heat flux density q_i . The Cu-resistance thermometer indicates a mean temperature T_i of the copper at this initial condition . Because of the carbon thermometer location, and the rather large q_i-values in post-quench regime C, the carbon resistance thermometer will have a larger T_i-value. However this signal of the carbon thermometer is less sensitive to T-changes . Consequently, the Cu-thermometer is more reliable and more accurate during the initial phase of the cooldown from post-quench regime C.

In post-quench regime B the efficient cooldown permits rather fast changes of T with time t .Therefore, the transients recorded by the thermometer may not be representative of a uniform cooldown process. In post-quench regime B however , film boiling prevents a fast cooldown to the superconducting state. The specimen mass is large enough to cause a rather slow temperature decrease during the film boiling process in post-quench regime C. Therefore, this regime will provide the largest contribution to the entire cooldown time (designated as τ). The complete recovery of all type II filaments may take a much longer time than the recovery of 50 % of the filaments. In order to obtain a reasonably defined time, the recorded value at establishment of $R_o/2$ (50 % of the residual resistance) has been utilized as τ. We turn first to data of single specimens.

Single Specimens . The individual specimen IS-1 was employed to find τ for formvar-coated samples. Subsequently, after removal of the formvar , IS-4B provided data. Figures VI.1 and VI.2 show the potential difference of the Cu-thermometer (and composite respectively) versus time t. Figure VI.1 pertains to post-quench regime B with T_i -

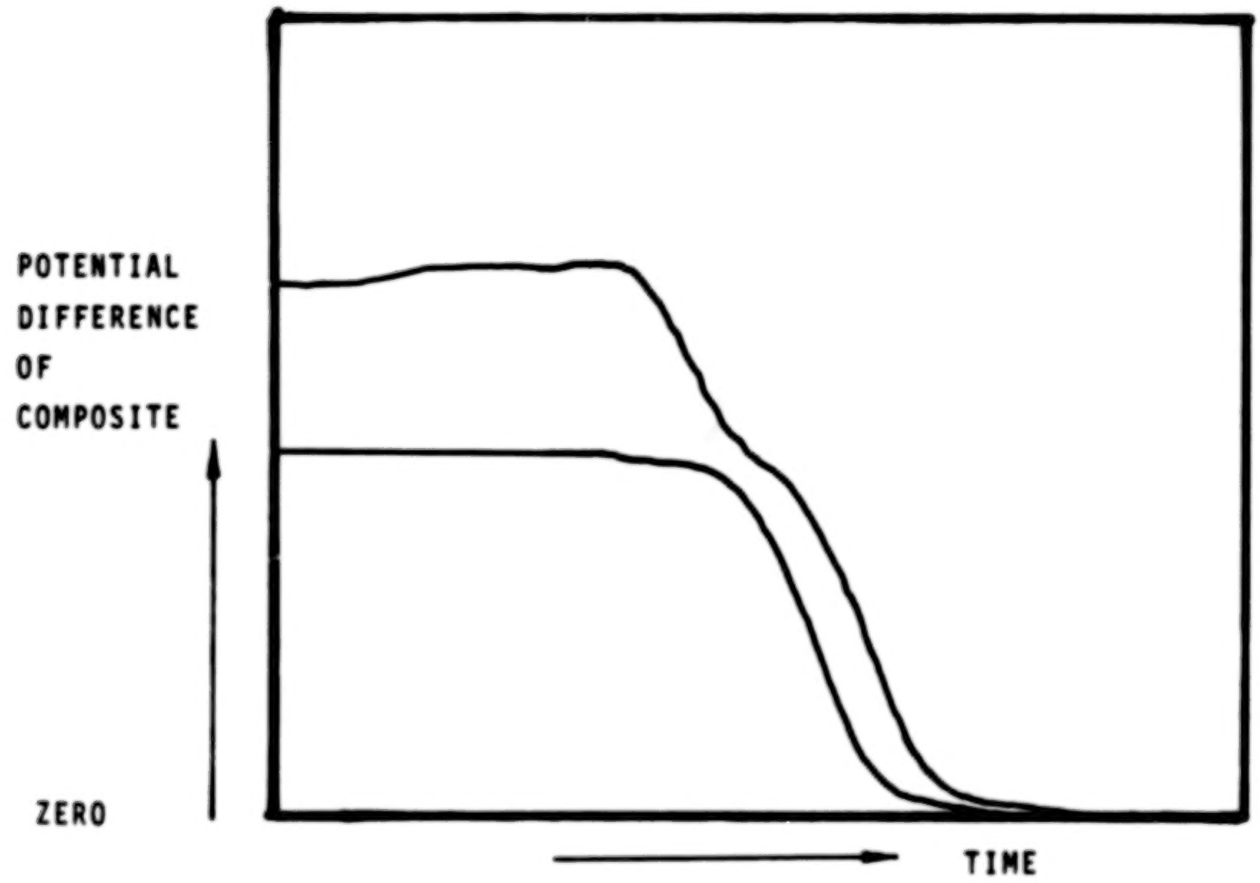

Figure VI.1 . Cooldown of formvar-coated specimen IS-4 from post-quench regime B ; T_b = 3.0 K

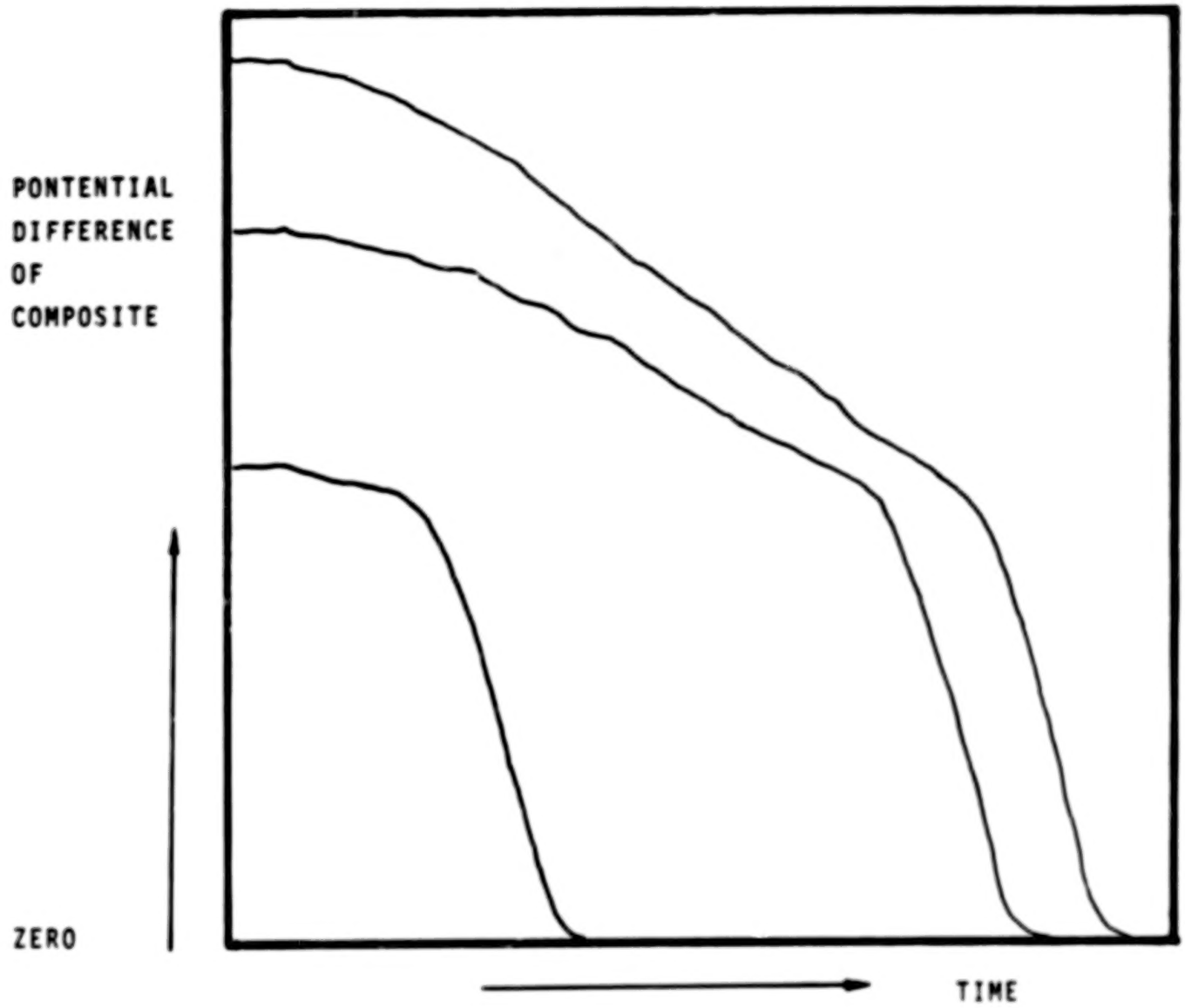

Figure VI.2 . Cooldown of formvar-coated specimen IS-4 from high initial temperatures T_i ; T_b = 3.0 K

values in the nucleate boiling range of He I , or in the Kapitza resistance - dominated range in He II. Figure VI.2 has relatively high T_i-values in post-quench regime C with initial film boiling conditions.

Figure VI.1 displays one resistance - time curve R(t),shown as potential difference of the Cu-thermometer, with a low initial resistance R_i and one single "S". On the upper curve two S - shaped portions show up. The lowest initial resistance corresponds to T_i just above the insensitive range of the Cu-thermometer. In this range the temperature changes from about 25 K to T_{sn} with a very small variation in R. At T_{sn} the recovery of the superconducting state is initiated. Subsequently, at the middle of the S-shaped trace a resistance of about 50 % of the residual value R_o is reached. After this point of a large derivative dR/dt ,the rate of change of R with time is decreasing again, and eventually the bath temperature is recovered.

The upper trace in Figure VI.1 appears to have two S-shaped portions resulting from two different phenomena. In the first "high" temperature range the variation of the temperature with time is indicated clearly. In the second portion the change of the electrical resistance toward zero is shown. At high values of R the initial change dR/dt appears to be quite rapid. The subsequent decrease of dR/dt is not necessarily an indication of a drastic change of dT/dt because of the cooldown in the insensitive region from 25 K to T_{sn}. The subsequent recovery of the superconducting state seems to differ but little from the first curve discussed above.

Figure VI.2 has one record for a rather low initial value of R_i compared to the other two curves. At low R_i only a short film boiling time interval is seen in the record. Subsequently a rather large dR/dt occurs in all traces. As R_i , and with it T_i , is raised the time interval of film boiling is prolonged. For the highest R_i in Figure VI.2 the contribution of film boiling to $\bar{\alpha}$ is dominant . The film boiling value of the heat transfer coefficient h_{if} is small. This causes a slow

cooldown process at high T with quasi-steady transport conditions of film boiling. Another feature of the runs in Figure VI.2 is a nearly constant temperature at which the change in derivative dR/dT occurs . This particular property has been seen also in studies of room temperature liquids (as reported for instance in Reference 26 and related work) .

Figure VI.3 plots the cooldown time τ versus the initial temperature T_i . This figure includes both, the coated specimen (IS-3) , and the bare conductor (IS-3B). Low cooldown times result when T_i remains in the lower range of the post-quench regime B . As T_i is raised from these small values, τ starts to rise from the order of magnitude 100 milli-seconds to the order 1 s . The time τ is seen to be a monotonically increasing function of T_i in Figure VI.3 . In this plot however the data scatter prevents a clear distinction between data of different post-quench regimes . Furthermore , a clear assessment of the coating effect appears to be difficult . Within data scatter the insulating formvar layer does not appear to cause increased cooldown times. In fact, some of the data indicate even lower τ-values for the coated sample.

Figure VI.4 permits a more detailed recognition of the influence associated with the two post-quench regimes B and C . The time τ is shown as a function of the initial heat flux density q_i for various bath temperatures. Details of the symbols used are contained in Table VI.I. The function for the bath temperature T_b = 4.2 K is roughly in the middle of the graph. There is a clear change in the derivative $d\tau/dq_i$ at a certain q_i-value, and a related "jump" in τ . A closer inspection of the discontinuity in slope shows a continuation of the upper branch of τ to a minimum value which corresponds to the minimum heat flux (referred to sometimes as "Leidenfrost point"). In order to reach this point we have to raise q_i first into regime C and lower it subsequently to the lowest possible value of q_i . On the lower branch for τ the highest q_i-value attainable is q_p .

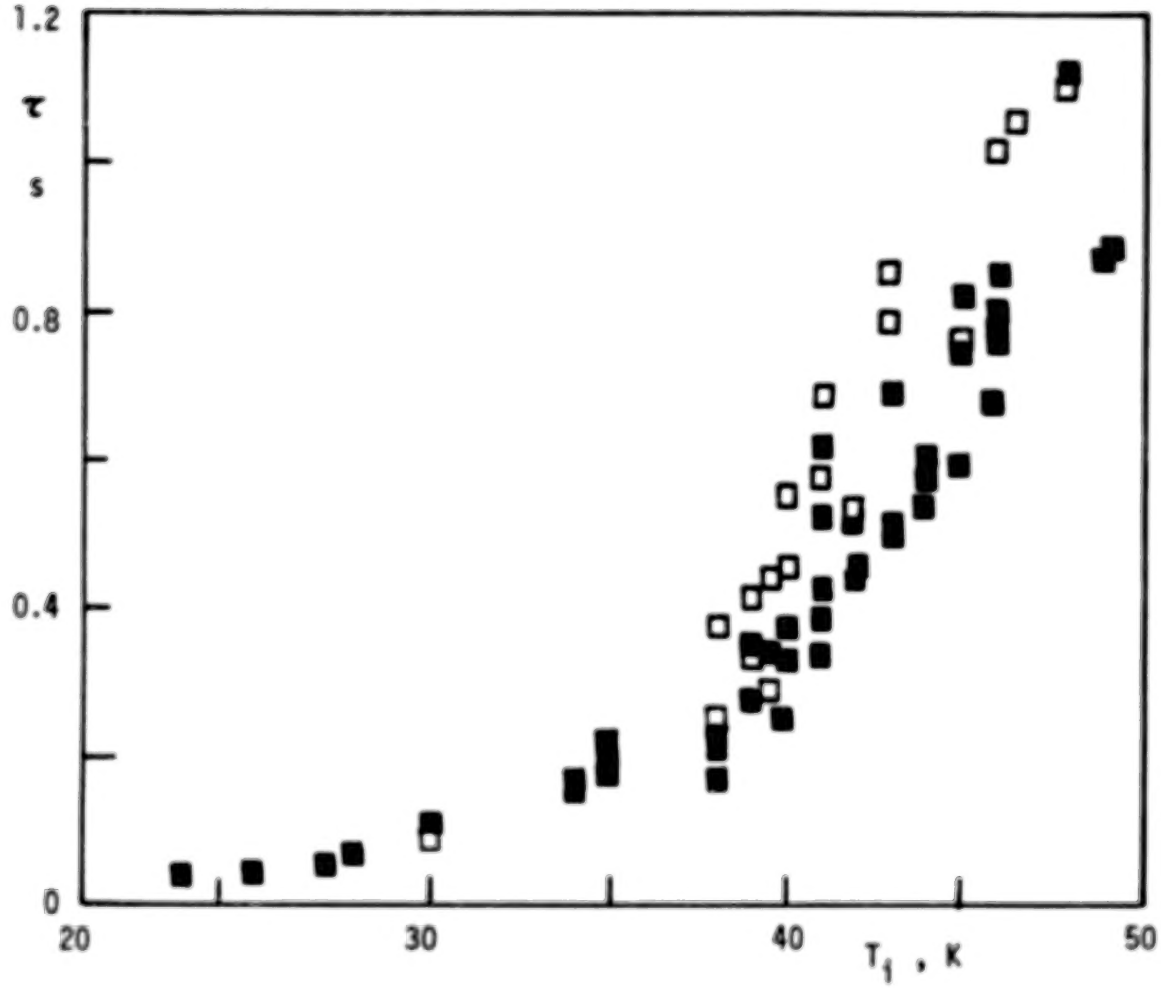

Figure VI.3 . Cooldown time as a function of the initial temperature T_i
(Open sqaures : Bare sample IS-4B; Full squares: Coated sample IS-4)

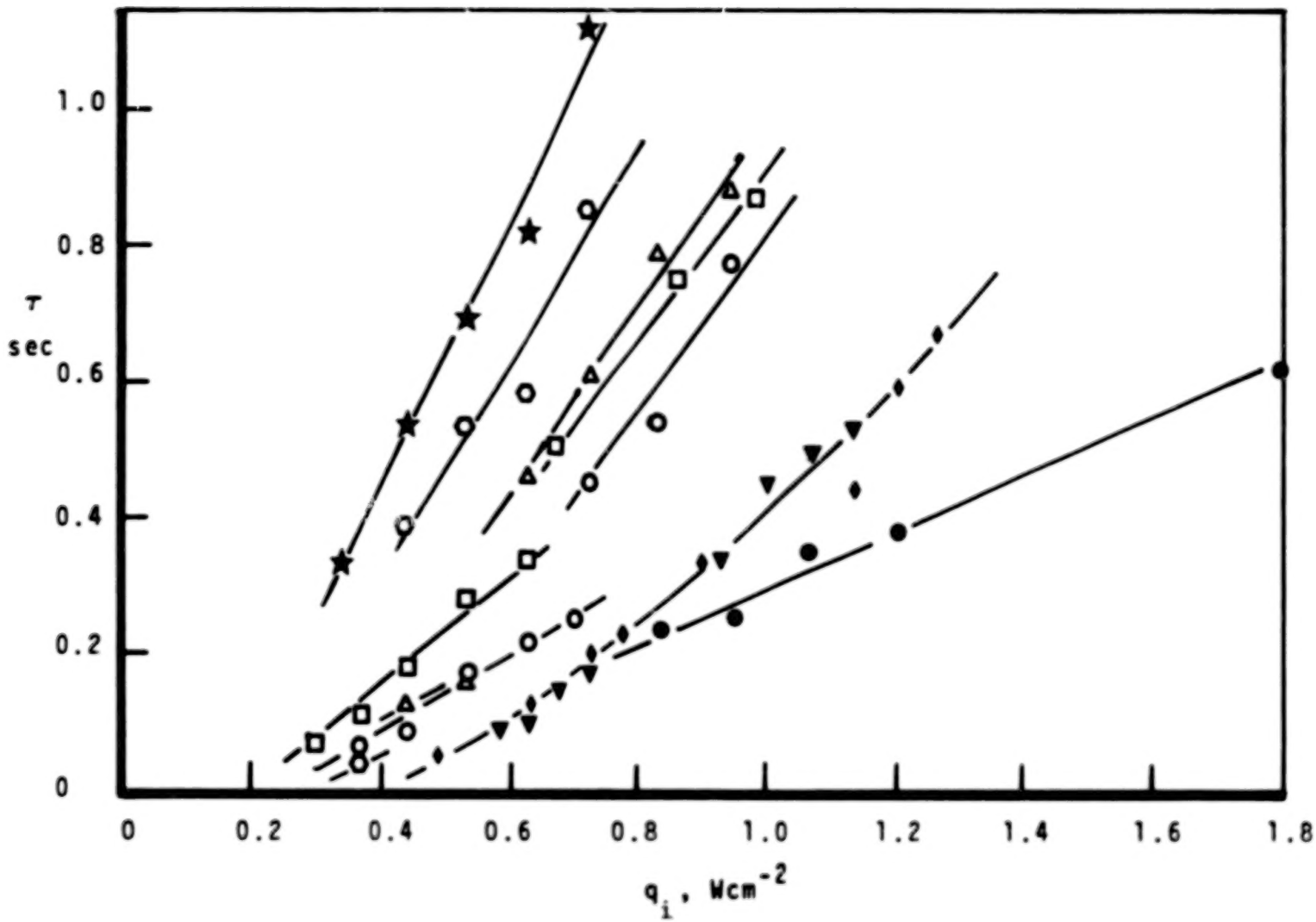

Figure VI.4. Cooldown time as a function of the initial q_i- value for various T_b (Table VI.I)

SYMBOLS	BATH TEMPERATURE K
□	4.20
○	3.50
△	3.00
○	2.50
★	2.20
▼	2.160
♦	2.140
●	2.130

TABLE VI.1 . Symbols used in Figure VI.4 for single specimens IS-4 and IS-4B

The influence of the bath temperature T_b in Figure VI.4 is quite distinct in the He I regime. As T_b is lowered, the time τ at a specified q_i-value in regime C increases significantly until the lambda temperature is reached. In the He II regime a sharp drop in τ occurs. The data however pertain primarily to post-quench regime B , (as q_p is quite large).

The strong variation of τ with T_b is seen more clearly in Figure VI.5 which plots the cooldown times for a specified q_i -value . The various functions τ (T_b) at constant initial heat flux density exhibit a minimum of τ in the He I range between 3 and 4 K . The high τ-values of the minimum all are in the post-quench regime C (film boiling). Low values of τ pertain to post-quench regime B. In between there is a range of τ in which the switch from regime B to C takes place . Low τ-values of these intermediate curves belong to post-quench regime B.

In the He II range of temperatures Figure VI.5 shows a rather steep decrease of τ as T_b is lowered from the He I side of the lambda transition to the He II side. The He II data indicate that τ decreases below the order of magnitude 100 milli-seconds outside of the lambda point vicinity. This drastic decrease of the cooldown time however is obtained only in post-quench regime B.

Cooldown of the conductor bundle was observed also at various bath temperatures in near-saturated liquid He^4 . The cooldown times obtained are shown in Figure VI.6 as a function of q_i for various T_b -values. It appears that three-dimensional effects influence in part the results for τ. As most of the data had been taken in post-quench regime B , the majority of τ-data is relatively low (compared to Figure VI.4).

It is concluded that for both types of the specimens , the bundle and the single conductor, He II permitted a rapid recovery of the superconducting state. In addition , the formvar coating did not show any detrimental effects, as far as the range of the present τ-data is concerned.

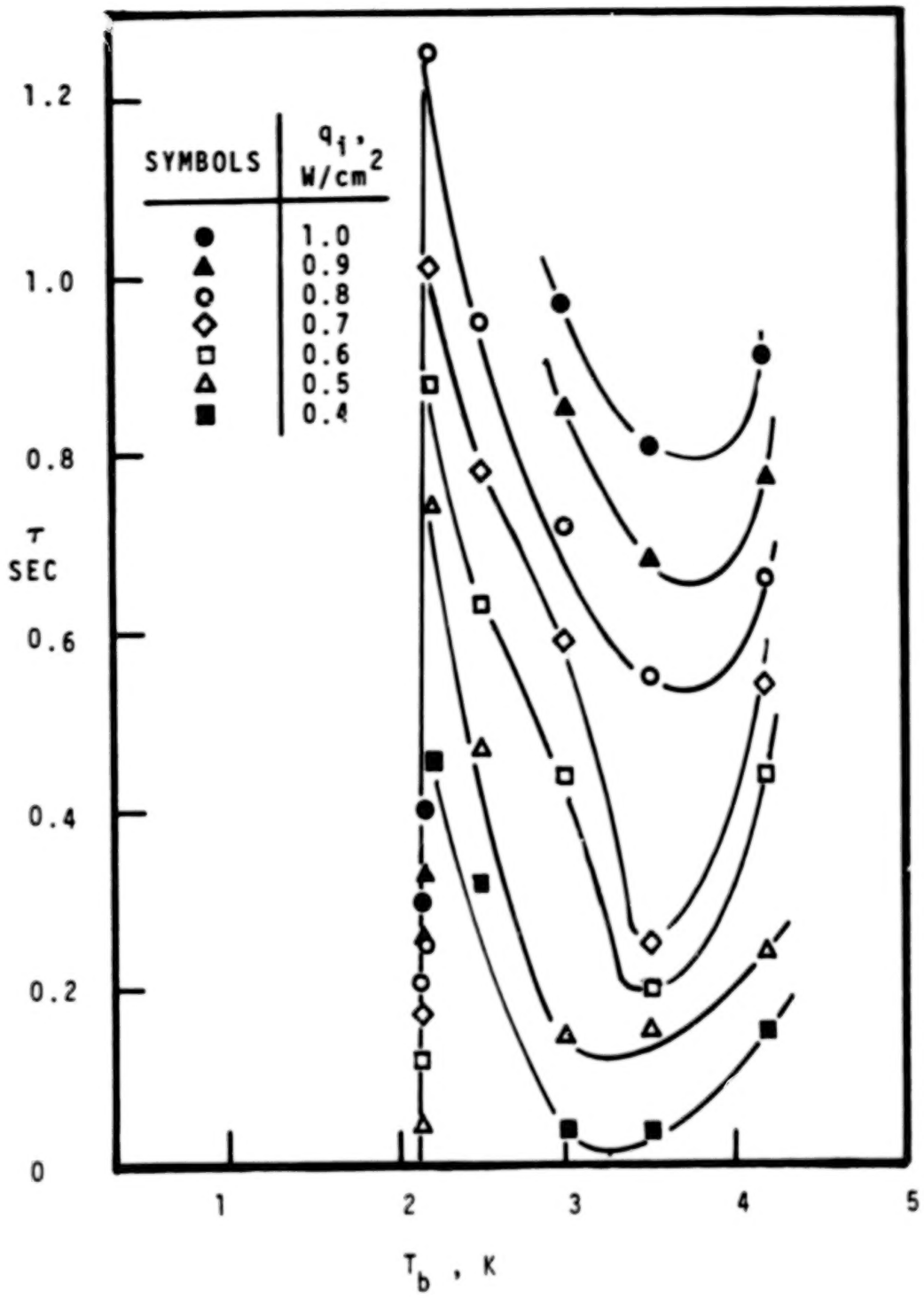

Figure VI.5 . Cooldown times of specimen IS-4 versus bath temperature T_b

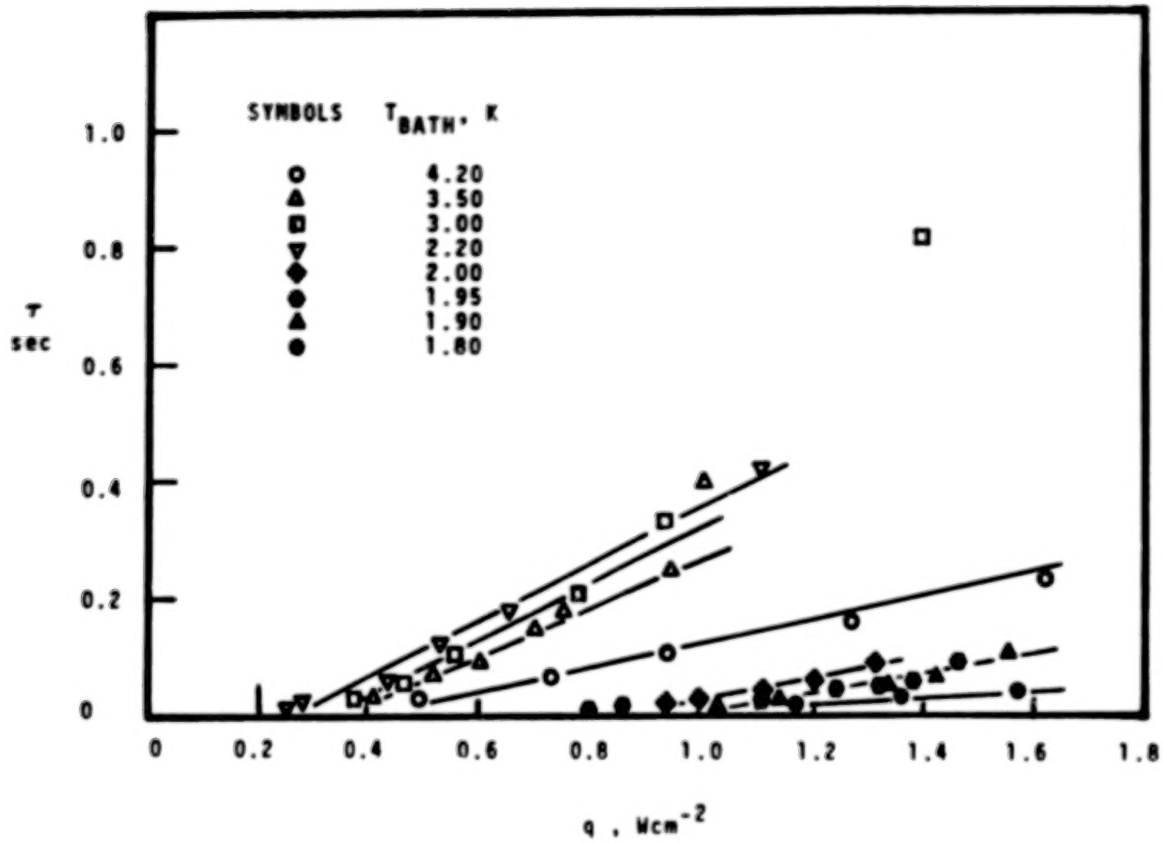

Figure VI.6. Cooldown times of composite conductor bundle

VII. FORCED FLOW EFFECTS

In view of several attractive properties of the coolant He II, forced flow has been investigated primarily at elevated pressures and at temperature T_b of bulk He II below the lambda temperature. These studies have been conducted with a different heater simulation geometry (using normal metal components only). (This work has been carried out on the basis of NSF-supported studies of supercritical He^4 with emphasis on He II). The insulated apparatus had the shape of a U-frame with a central heated section, made out of Cu, in the middle of the "U". For details of the apparatus we refer to Reference 30 and related work. In this Section VII we outline briefly major results obtained, and start first with a comment of the influence of the pressure (P) on the Kapitza conductance.

Early work of Challis, Dransfeld and Wilks (Reference 27) has been concerned with $h_{if}(P)$ of a copper- He II boundary. The Kapitza conductance h_{if} increased but little with P. Most of the data however were below or near the temperature of the upper triple point of solid-He II-He I coexistence. The only run above this temperature showed nearly no change $h_{if}(P)$ at all. In early investigations of single specimens Madsen and McFadden (Reference 28) found a noticeable increase of h_{if} (at constant T_b) with respect to the data for near-saturated He II. Recently, van Sciver and Boom reported data in Reference 29 for an aluminum surface. It appeared to be difficult to evaluate an exact value of $(dh_{if}/dP)_{T_b}$. However the data for higher pressures always appeared to exceed those for near-saturated He II at low pressure.

The U-frame data discussed in this Section VII appear to agree with these various literature findings. The present h_{if}-data for the Kapitza conductance are overall heat transfer coefficients including additional thermal resistances. Figure VII.1 presents an example for a constant bulk fluid temperature $T_b \approx 1.95$ K and $P > P_c$. No distinct mass flow rate influence appears to be present within data scatter. Similarly, the pressure influence is quite weak, and an evaluation of the

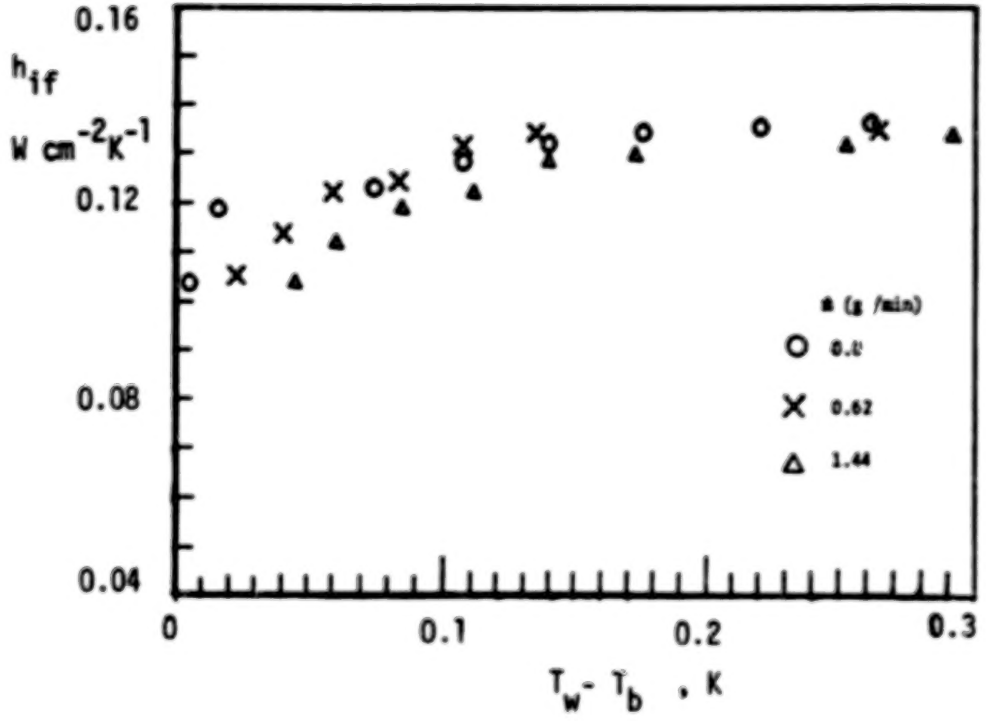

Figure VII.1 . Overall Kapitza heat transfer coefficient at T_b= 1.950 K and a pressure P = 2.4 bar (from Reference 30)

derivative $(dh_{if}/dP)_{T_b}$ faces similar difficulties as in Reference 29. Details of the U-frame studies are contained in Reference 30 . Figure VII . 3 includes Kapitza conductance results and the related data for phenomena involving He I- He II two-phase transport above the thermodynamic critical pressure ($P > P_c$).

Figure VII.2 presents data primarily in the single-phase regime of supercritical He II during Gorter-Mellink flow in the U-frame. The heat flux density q is displayed as a function of the difference between the wall temperature T_w and the bulk fluid temperature.In contrast to the data for single specimens, the quantity q is related to the duct cross section . The mass flow imposed externally appears to exert a negligible influence on the single phase transport. Even at the transition to two-phase conditions no mass flow effect shows up in the range of $\dot{m}$ covered in the runs.

Figure VII.3 however shows that there are distinct effects of $\dot{m}$ on the transport rates in the He I- He II regime. The overall heat transfer coefficient has been normalized in terms of the Kapitza value $(h_{if})_o$ in the single phase regime. The temperature difference between wall and bulk fluid temperature has been expressed as ratio $(T_w-T_b)/(T_\lambda - T_b)$. As the reference difference from T_b to T_λ is so small , the two -phase regime (He I - He II) is characterized by large ratios of the temperature differences.

Figure VII.4 shows q in the range of temperatures in which superconductivity of NbTi is possible. In the two-phase regime the mass flow rate has a strong effect on the coolant's effectiveness. This is interpreted as a significant thinning of the He I layers which have formed at the "hot" location near the heater , when $\dot{m}$ is raised.

As the temperature of the pressurized bulk fluid He II is changed, from the vicinity of the lambda transition to 1.95 K, there is a strong effect of T_b in the range of interest for superconductivity of NbTi. Figure VII.5 indicates that there are significant differences during both the transition process , and during established He II- He I two-

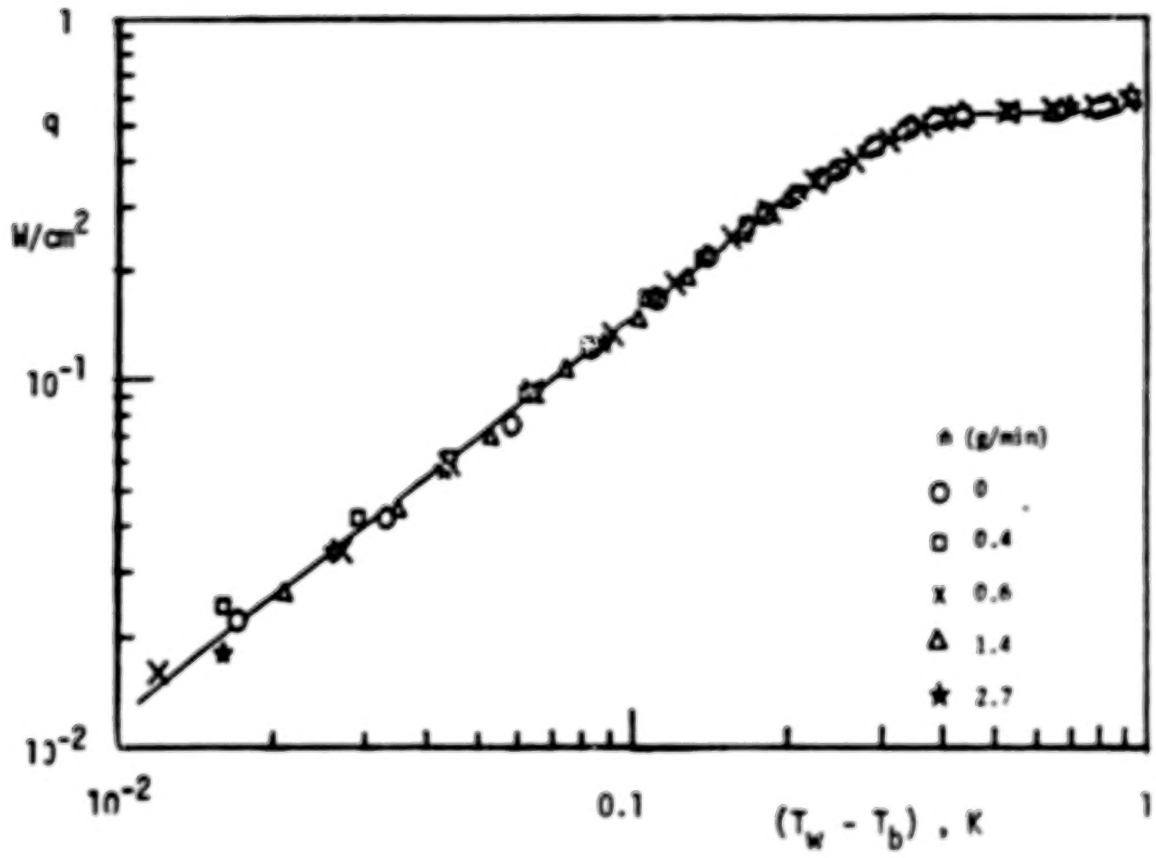

Figure VII.2.Heat flux densities q above the thermodynamic critical pressure;
P = 4.0 bar ; T_b = 2.05 K ; (from Reference 30)

BLANK PAGE

BLANK PAGE

TABLE OF CONTENTS

	Page	
I. SUMMARY	1	1/A6
II. INTRODUCTION	3	1/A8
III. COMPOSITE CONDUCTOR PROPERTIES , SPECIMENS , AND EQUIPMENT	5	1/A10
IV. QUENCH REGIMES OF SINGLE SPECIMENS AND RELATED RESULTS	13	1/B4
V. QUENCH ONSET OF THE CONDUCTOR BUNDLE AND RELATED PHENOMENA	46	1/E10
VI . COOLDOWN OF COMPOSITE CONDUCTORS FROM POST-QUENCH CONDITIONS	55	1/F6
VII. FORCED FLOW EFFECTS	66	1/G8
VIII. CONCLUSIONS	74	2/A7
APPENDIX A . EXPERIMENTAL DATA	80	2/A13

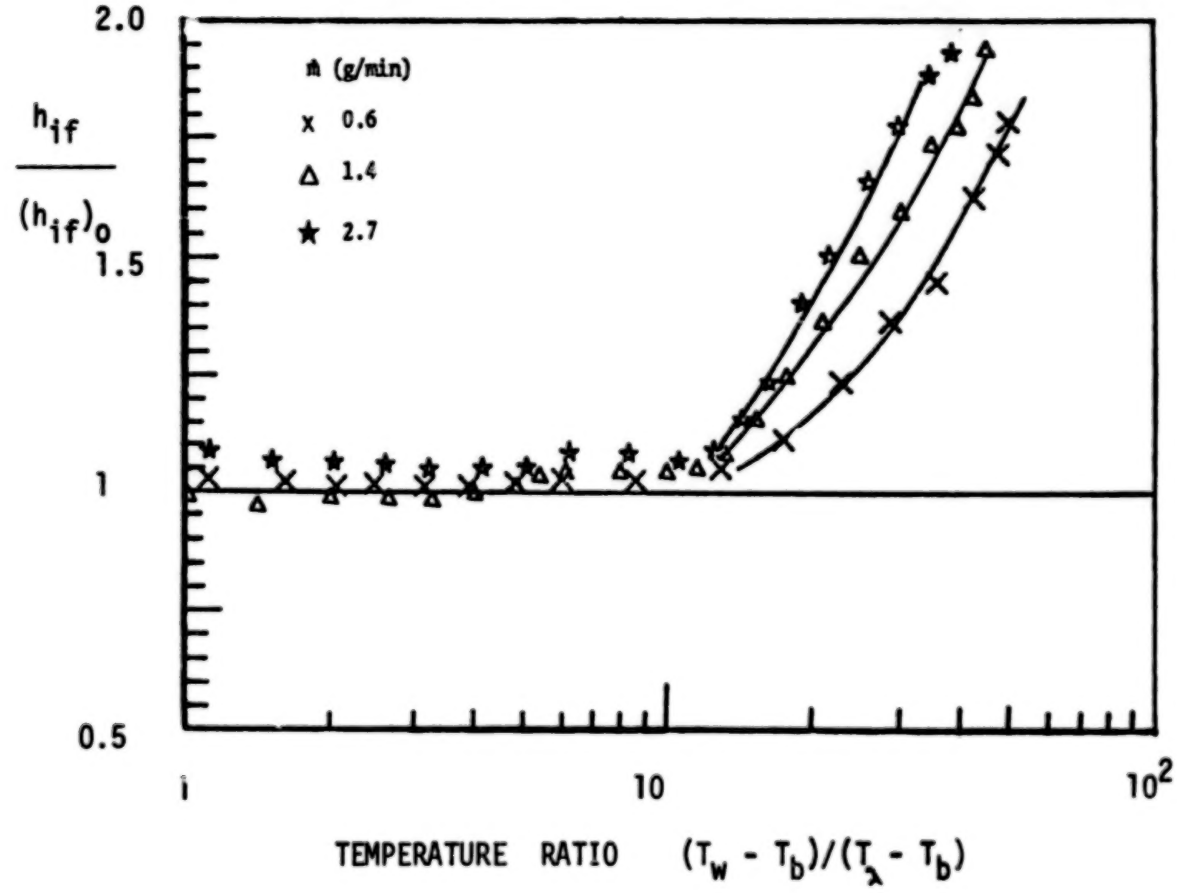

Figure VII.3 . Overall conductance ratio versus temperature ratio for He I- He II two-phase motion ; T_b = 2.05 K ; P = 2.4 bar; (From Reference 30)

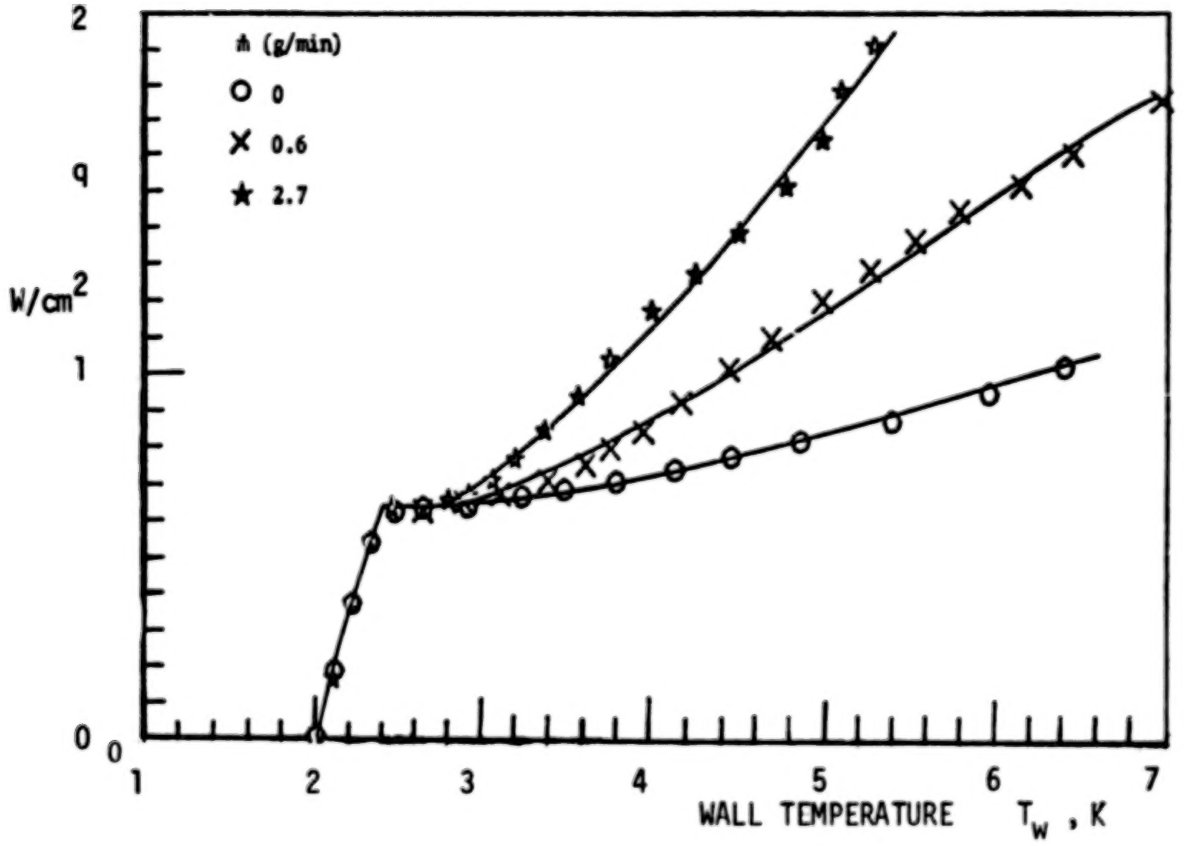

Figure VII. 4. Heat flux density q of two-phase motion (HeI-He II) at supercritical pressure P = 6.7 bar ; (T_b = 2.00 K); Abscissa : Wall temperature T_w; (Results from Reference 30)

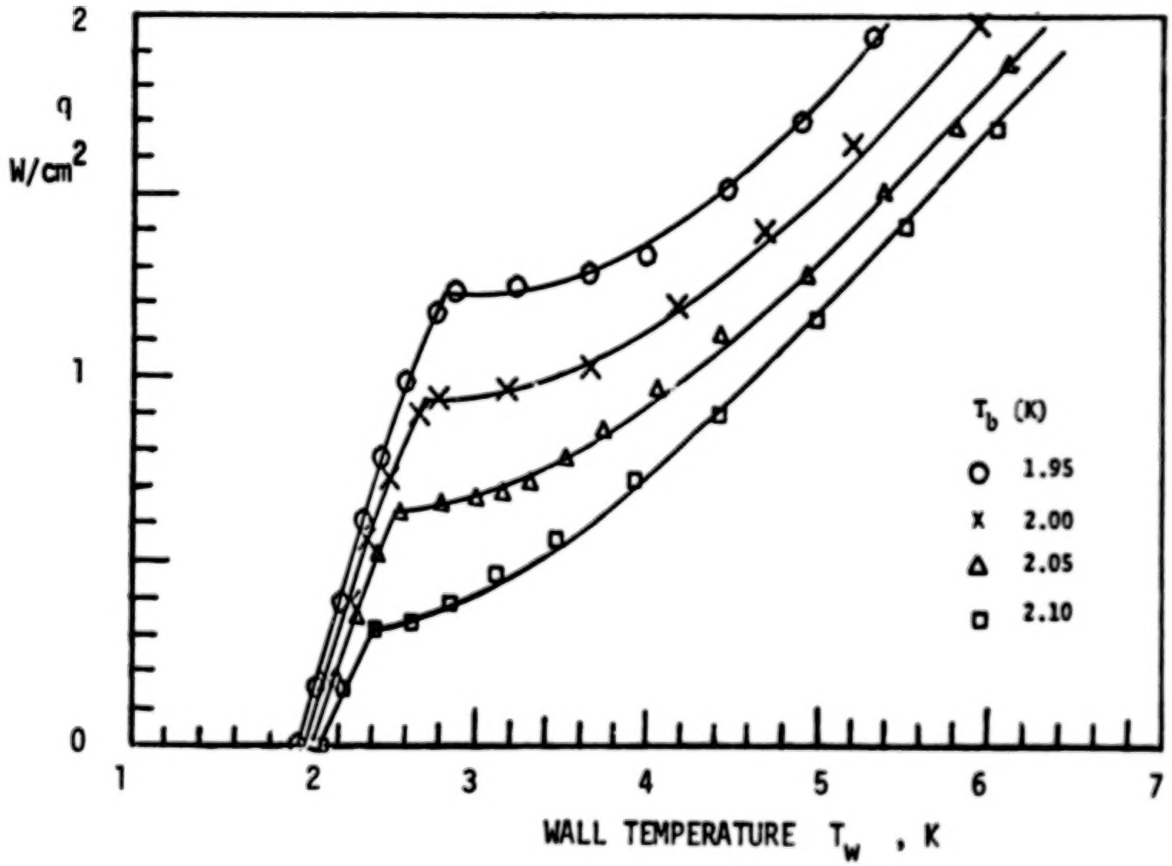

Figure VII.5 . Influence of bulk fluid temperature T_b on heat flux densities q in the two-phase regime (He I- He II) above the critical pressure; P = 2.4 bar; Mass flow rate $\dot{m}$ = 1.4 g/min ; (Data from Reference 30)

phase motion. As the temperature is raised more in the two-phase regime the effect of T_b appears to weaken somewhat. It is this region however which appears to permit rather large changes in the cooling conditions of the pressurized two-phase fluid system.

In recent time piston-induced forced flow studies have become known which appear to permit "quenching" of superfluidity in the single phase regime. These results reported in Reference 31 and Reference 32 have been discussed with respect to implications for large scale equipment . Velocities of the order 10^2 cm/sec have been inserted to illustrate the "normal " state of the fluid. As the Reynolds number of the forced flow is quite high and significantly above the superfluid threshold values , no problems with piston or turbomachine operation appear to be caused by any fluid-dynamic superfluidity. In the present U- frame investigations however very small velocities have been applied without pumping on the He II directly. Therefore, the thermomechanics of Gorter-Mellink flow is disturbed insignificantly in the single-phase regime. Further, the velocities , despite their smallness, are beneficial enough to aid significantly in the two-phase regime. Therefore, implementation of this mode of motion inside the ducts of a He II-cooled magnet system appears to retain many of the benefits of He II operation established during the studies summarized in the previous sections.

For many details of the U-frame studies we refer to Reference 30 and related work.

VIII. CONCLUSIONS

The present conclusions pertain to both, the first phase and the second phase of the investigations . The results of quasi-steady runs , and data for recovery from "high" temperatures (e.g. 40 K), show that coatings are important components for composites used in certain magnet categories. The class of magnets under consideration incorporates a stabilizer design which is based on the use of the latent heat of vaporization of liquid He^4 . This implies that the pressure range under consideration for the coating application extends from saturated liquid to the vicinity of the critical point. Temperatures range all the way from He II states (about 2 K) to the vicinity of the thermodynamic critical temperatures of He^4 .

Quasi-Steady Runs. From quench experiments with insulated and uninsulated specimens the following conclusions are drawn:

1. The ratio of the thickness of the coatings d_{FV} to the thermodynamic limiting thickness δ_L is a governing parameter which influences the quench behavior noticeably.The thickness δ_L is a strong function of temperature.
2. Thin coatings, characterized by $d_{FV}/\delta_L < 1$, show the quench behavior known from "bare" conductors. Also the case $d_{FV} = \delta_L$ exhibits this behavior . Accordingly, in the parameter range covered in the present runs, the phenomena of bare conductors are not altered.
3. Thick coatings , characterized by $d_{FV}/\delta_L > 1$ push the fluid phase transition to high metal temperatures. In other words , the quench onset is no longer coupled to interactions caused by the peculiar transitions of "boiling curves" of He^4 .
4. The quantification of coating effects is conveniently displayed in a "quench diagram" which contains various

pre- and post-quench regimes.

For easy reference the quench diagram of Section IV for the present MHD - conductor is shown schematically as simplified Figure 8.1. The two heat flux densities , q_o for the quench onset, and q_p for take-off toward high temperatures, generate three regimes : Pre-quench regime A , post-quench regime B with solid-liquid contact , and post-quench regime C with liquid contact eliminated due to the presence of the Leidenfrost gas film. Thick coating conditions are generated always when post-quench regime B exists . Thin coating conditions are generated on the He I side in the lambda point vicinity, and near the thermodynamic critical temperature. Thick coating conditions prevail in a broad quench regime B between 3 and 4 K , and in liquid He II.

Comparing the single specimen with the bundle of conductors we note similar effects. However the thin coating regime of the bundle has been found to be slightly enlarged, and the thick coating range turned out to be narrowed down in He I . No effects of this nature have been seen in superfluid liquid He II.

Recovery Time Results. The present studies of cooldown from post-quench conditions confirmed the existence of the quench diagram as a significant classification scheme . The following conclusions pertain to the times needed for recovery of superconductivity :

I. Coated specimens show a fast cooldown due to the displacement of the boiling mode transition to higher metal temperatures . This comparison pertains to a constant initial metal temperature, and it is required that the maximum metal temperature with liquid-solid contact is not exceeded.

II. A minimum in the recovery time is obtained when the parameter d_{FV}/δ_L has the highest value ,e.g. between 3 and 4 K in He I,and around 2 K in He II .

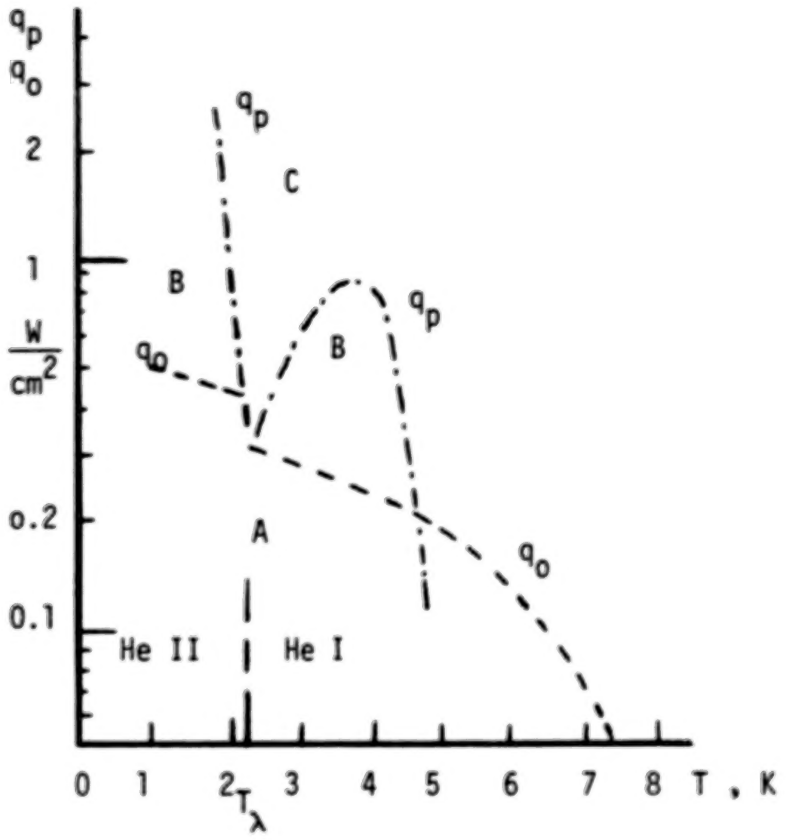

Figure 8.1. Quench regimes (schematically)

q_o = Quench onset function: Heat flux density for coated conductors with thick coatings characterized by $d_{FV}/\delta_L > 1$;

q_p = Take-off function: "Peak"value of the heat flux density (last point prior to incipient film boiling);

Regimes

A Pre-quench

B Post-quench regime created by thick coatings with $d_{FV}/\delta_L > 1$;

C Post-Quench regime with gas film around conductor; C is the usual case of post-quench conditions for bare conductors, or coated conductors with "bare" behavior $d_{FV}/\delta_L < 1$.

III . Cooldown from very high metal temperatures in post-quench regime C is dominated by the existence of the gas film around the quenched specimen . Its contribution to the recovery time is the major factor. Nevertheless , the data for coated specimens show times slightly <u>below</u> bare conductor data. These results tend to confirm findings known for higher temperatures (e.g. Ref.33).

There are three additional aspects: The use of He II, the choice of the system pressure, and the matching of disturbance spectra with the coating selection.

When He II is selected, the possibility of a small coating layer thickness and high dielectric strength appears to be a most desirable goal, as the ratio d_{FV}/δ_L may stay above unity in a larger range than for other liquid conditions. The major criterion should not be overlooked: He II is most attractive <u>after</u> other system design preferences have led to the choice of low temperatures on the basis of enhanced superconductivity parameters (e.g. critical current density).

The <u>pressurized</u> fluid system has general and specific advantages for He II , be it a classical refrigeration system , or a novel He II-He I hybrid system, as pointed out previously (Ref. 34). This choice involves : a. Leakage of He^4 <u>out</u> of the system (not into it), and b. Improved dielectric strength.

Concerning the third point, the matching of disturbance spectra with the coating selection requires more information on dissipative phenomena, including magneto-mechanical behavior, of the present MHD-conductor winding scheme.

REFERENCES

1. Caspi, S.,Lee, J.Y.,Kim Y.I., Allen R.J., and Frederking, T.H.K., Report NASA CR 2963, April 1978; (UCLA-ENG-7767)
2. Green, M.A., Burns, W.A., Eberhard, P.H., Gibson, G.H., Miller, P.B., Ross, R.R., Smits, R.G. and Taylor, J.D.,7th Intern. Cryog. Eng. Conf. London 1978, paper 2M-4
3. Bon Mardion, G., Claudet, G., Seyfert, P., and Verdier, J., Adv. Cryog. Eng. Vol. 23, p. 358, 1978
4. Caspi, S., Chang, Y.W.,Lee, J.Y. and Frederking, T.H.K., Report UCLA-ENG-76109 , 1976
5. Matsumoto, D.S. , Reynolds, C.L., and Anderson, A.C., Phys. Rev. Vol. B 16, p.3303, 1977
6. Hust, J.G., Cryogenics , Vol. 15, p.8 , 1975
7. Schmidt, Phys. Rev. Vol. B 15, p. 4187, 1977
8. Haben R.L., Madsen, R.A., Leonard, A.C., and Frederking, T.H.K., Adv. Cryog. Eng., Vol. 17, p. 323, 1972
9. Amar, R.C., Ph.D. thesis, University of California, Los Angeles 1974
10. Leonard, A.C. and Clermont, M.A., Proc. 4th Intern. Cryog. Eng. Conf., PIPC. Sci. Technology Press Ltd.,London,p.301,1972
11. Soloski, S.C., Ph.D. thesis, University of California, Los Angeles 1977
12. Rohsenow, W.M., in Frost, W , (Ed.), Heat Transfer at Low Temperatures", Plenum Press, New York, 1975, p. 107
13. Lyon, D.N.,Int. Adv. Cryog. Eng.,Vol. 10, p. 371, 1965
14. Schmidt, C., Appl. Phys. Letters , Vol. 32, p. 827, 1978
15. Sydoriak, S.G. and Roberts, T.R., J. Appl. Phys.,Vol. 28,p.143, 1957
16. Sydoriak, S.G. and Roberts, T.R., Liquid Helium Technology , Pure and Appl. Cryogenics , Vol. 6, Pergamon 1966, p. 115
17. Linnet, C. and Frederking , T.H.K., Wärme- und Stoffübertragung, Vol. 5, p.141 , 1972
18. Guggenheim, E.A. , J. Chem. Phys., Vol. 13, 253 , 1945
19. Narsimhan, G., Brit. Chem. Eng. , Vol. 12, 897 , 1967
20. Defay, R., Prigogine, I., and Bellemans, A., Surface Tension and Adsorption, Wiley , New York , 1966, p. 156
21. Alamgir, Md., and Lienhard, J.H., Trans. ASME, J. Heat Transfer, Vol. 100, p. 324, 1978
22. Hsu,Y.Y., and Graham, R.W., Transport Processes in Boiling and Two-Phase Flow Systems, McGraw-Hill, New York, 1976

23. Wilson, M.N., Liquid Helium Technology, Pure and Appl. Cryogenics, Vol. 6, Pergamon Press 1966, p. 109

24. Purdy, V., Frederking , T.H.K., Boom, R.W., Guderjahn, C.A. Domoto, G.A. and Tien, C.L., Adv. Cryog. Eng. Vol. 14, p. 146 , 1969

25. Chen, W.Y. and Purcell, J.R., J. Appl. Phys. Vol. 49, p. 3546, 1978

26. Dhir, V.K., and Purohit, G.P., Nucl. Eng. and Design, Vol. 47, p. 49, 1978

27. Challis, L.J., Dransfeld, K., and Wilks, J., Proc. Roy. Soc. A, Vol. 260, p. 31, 1961

28. Madsen, R.A. , and McFadden, P.W., Adv. Cryog. Eng., Vol. 13, p. 617, 1968

29. Van Sciver, S.W. and Boom, R.W., Heat Transfer from Aluminum to He II , paper ASME 78-HT-51, May 1978

30. Caspi, S., Ph.D. thesis , Univ. California, Los Angeles, 1978

31. Johnson, W.W. and Jones M.C., Adv. Cryog. Eng., Vol. 23, p.363, 1978

32. Johnson, W.W., and Jones, M.C., Measurements of Combined Axial Mass and Heat Transport in He II, NBS Techn. Note 1002, Febr. 1978

33. Maddox, J.P. and Frederking, T.H.K., Adv. Cryog. Eng. Vol. 11, p. 536, 1966

34. Caspi, S., Lee. J.Y., Soloski, S.C., and Frederking, T.H.K., Rept. UCLA-ENG-7713, Univ. Calif. Los Angeles, January 1977

APPENDIX A. EXPERIMENTAL DATA

Table A.I

RESULTS FOR FORMVAR-COATED SPECIMEN IS-4 (NEAR-SATURATED LIQUID He^4)

q_p peak heat flux density at onset of film boiling in post-quench regime C

q_r recovery values of the heat flux density for $dq < 0$ at cessation of film boiling

q_o q-value at quench onset of superconductor

T_b K	q_p W/cm^2	q_r W/cm^2	q_o W/cm^2
4.20	.936	.800	.237
4.20	.890	.767	.237
4.014	.936	.833	.274
3.800	.947	.800	.268
3.600	.866	.790	.274
3.400	.806	.721	.286
3.200	.746	.664	.300
3.05	.705	.551	.327
3.00	.705	.569	.313
2.800	.587	.489	.330
2.600	.515	.428	.327
2.400	.436	.343	.334
2.350	.417	.325	.341
2.300	.392	.313	.334
2.250	.380	.293	.313

Table A.I (Continued)

RESULTS FOR FORMVAR-COATED SPECIMEN IS-4

T_b K	q_p W/cm^2	q_r W/cm^2	q_o W/cm^2
2.240	.374	.290	.334
2.230	.375	.286	.334
2.220	.384	.284	.334
2.210	.370	.280	.330
2.200	.366	.275	.334
2.190	.365	.274	.334
2.180	.359	.267	.334
2.174	.377	.273	.334
$T_b < T_\lambda$			
2.164	----	----	.481
2.157	----	----	.498
2.124	2.60	----	.515
2.100	2.56	1.74	.506
2.045	3.61	----	.489
2.00			.515
1.90			.515
1.80			.533
1.70			.533
1.50			.524
1.33			.524

TABLE A.II

CONDUCTOR BUNDLE (FORMVAR-COATED):

OVERALL HEAT TRANSFER COEFFICIENTS AT QUENCH ONSET*)

SPECIMEN BS-1A

(SPACERS HORIZONTAL)

T_b, K	q_0, W/cm^2	$\bar{U}_0^{*)}$, W/cm^{2}K
4.20	.54	.12
3.00	.41	.073
2.20	.25	.039
2.16	.35	.054
2.15	.74	.12
2.13	.66	.103
2.11	.90	.14
2.07	1.0	.15
2.00	1.3	.19
1.9	1.3	.19

SPECIMEN BS-1B

(SPACERS VERTICAL)

4.20	.55	.13
3.00	.58	.10
2.16	.44	.069
2.13	.59	.092
2.10	.80	.12
2.00	1.16	.18

SPECIMEN BS-1A (SPACERS HORIZONTAL)

3.75	.40	.083
3.50	.36	.071
3.00	.37	.067
2.50	.32	.052
2.20	.25	.040
2.17	.29	.045
2.15	.40	.062

---

*) Based on diathermic area A_{tot} = 1.563 cm^2

TABLE A.III

COOLDOWN TIMES OF COATED SPECIMEN IS-4 AT VARIOUS BATH TEMPERATURES T_b FOR DIFFERENT INITIAL CONDITIONS (T_i,q_i) AND RECOVERY IN NEAR-SATURATED LIQUID

	INITIAL TEMPERATURE T_i, K	INITIAL HEAT FLUX DENSITY q_i, W/cm^2	COOLDOWN TIME τ, sec.
T_b=4.2K			
	28	.30	.070
	30	.37	.110
	35	.45	.180
	39	.53	.280
	40	.62	.335
	43	.67	.505
	46	.87	.750
	49	.98	.870
T_b=3.5K			
	27	.37	.060
	30	.45	.080
	34	.53	.175
	38	.62	.210
	40	.70	.250
	42	.72	.450
	44	.83	.540
	46	.95	.780

TABLE A.III . COOLDOWN TIMES of IS-4 (CONTINUED)

T_b=3.00K		
30	.45	.120
34	.53	.150
42	.62	.460
44	.72	.605
46	.83	.790
49	.95	.885
T_b=2.50K		
23	.37	.045
41	.45	.390
42	.53	.525
44	.62	.580
46	.72	.855
T_b=2.24K		
40	.30	.350
41	.37	.490
45	.53	.880
T_b=2.20K		
40	.34	.330
41	.45	.525
43	.53	.690
45	.62	.820
48	.72	1.12

TABLE A.III . COOLDOWN TIMES of IS-4 (CONTINUED)

T_b=2.16K

28	.58	.075
30	.62	.100
34	.67	.150
38	.72	.170
41	.924	.340
42	1.00	.450
43	1.07	.500
45	1.13	.535

T_b=2.14K

25	.49	.050
30	.62	.130
35	.72	.200
38	.78	.230
39.5	.89	.340
41	1.13	.435
45	1.20	.595
46	1.26	.670

T_b=2.13K

35	.84	.230
38	.95	.250
39	1.07	.350
40	1.20	.380
41	1.80	.620

TABLE A.IV

COOLDOWN TIMES OF UNCOATED SPECIMEN IS-4B AT VARIOUS BATH TEMPERATURES T_b FOR DIFFERENT INITIAL CONDITIONS (T_i, q_i) AND RECOVERY IN NEAR-SATURATED LIQUID He^4

	INITIAL TEMPERATURE T_i , K	INITIAL HEAT FLUX DENSITY q_i , W/cm^2	COOLDOWN TIME τ , SEC
T_b=4.2K			
	39	.62	.420
	41	.95	.580
	43	1.20	.790
	46	1.48	1.02
T_b=3.00K			
	39	.62	.340
	40	.95	.555
	43	1.33	.860
T_b=2.50K			
	40	.62	.460
	41	.83	.690
	48	1.26	1.10
T_b=2.15K			
	39.5	1.13	.285
	43	1.63	.530
	45	1.80	.740

1. Report No. NASA CR-3262	2. Government Accession No.	3. Recipient's Catalog No.
4. Title and Subtitle CRYOGENIC-COOLANT He^4-SUPERCONDUCTOR DYNAMIC AND STATIC INTERACTIONS		5. Report Date April 1980 6. Performing Organization Code
7. Author(s) S. Caspi, C. Chuang, Y. I. Kim, R. J. Allen, and T. H. K. Frederking		8. Performing Organization Report No. UCLA-ENG 7867 10. Work Unit No.
9. Performing Organization Name and Address University of California at Los Angeles Los Angeles, California 90024		11. Contract or Grant No. NSG-3153
12. Sponsoring Agency Name and Address National Aeronautics and Space Administration Washington, D.C. 20546		13. Type of Report and Period Covered Contractor Report 14. Sponsoring Agency Code

15. Supplementary Notes

Final report. Project Manager, James A. Burkhart, Wind and Stationary Power Division, NASA Lewis Research Center, Cleveland, Ohio 44135.

16. Abstract

Evaluation of a composite superconducting material (NbTi-Cu) has been continued with specific emphasis on favorable post-quench solid-cooling interaction regimes. Phase I of quasi-steady runs has been extended confirming the existence of a thermodynamic limiting thickness for insulating coatings. Investigations in the present phase II showed two distinctly different post-quench regimes of coated composites related to the limiting thickness. Only one regime, from quench onset to the "peak" value, revealed favorable coolant states, in particular in He II. Extension of the studies to transient recovery showed favorable recovery times from this post-quench regime (not drastically different from bare conductors) for both single coated specimens and a coated conductor bundle.

17. Key Words (Suggested by Author(s))	18. Distribution Statement
Low temperature coolant He^4; Heater simulation technique; Quench onset; Post-quench regimes for formvar-coated NbTi-Cu; Thermal conductances; Transient post-quench recovery; Recovery times	Unclassified - unlimited STAR Category 34

19. Security Classif. (of this report)	20. Security Classif. (of this page)	21. No. of Pages	22. Price*
Unclassified	Unclassified	88	A05

* For sale by the National Technical Information Service, Springfield, Virginia 22161

NASA-Langley, 1980

END

June 30, 1981